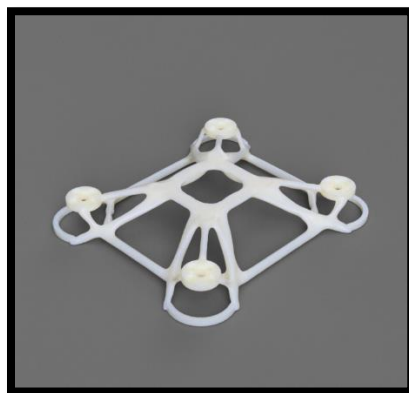


# Generative Design for 3D Printing of Advanced Aerial Drones



Toronto Metropolitan University  
(Formally Ryerson University)

The logo for Toronto Metropolitan University, featuring the text "Toronto Metropolitan University" in white on a blue rectangular background, with a yellow vertical bar to the right.

Toronto  
Metropolitan  
University

AER870 Aerospace Engineering Thesis

Samuel Osorio Marino

Dr. Kazem Fayazbakhsh

Last Reviewed: 2023-04-14

## Abstract

In the current study completed in the Facility for Research on Aerospace Materials and Engineered Structures (FRAMES), the feasibility of implementing generative design as a means of optimizing advanced aerial drone structures was explored. By conducting relevant literature review, theoretical investigations, and experimentation, generative design demonstrated its efficacy as a design tool for various engineering structure applications. Generative design uses a series of artificial intelligence (AI) algorithms to compute various potential geometries for optimized load distribution; it is a powerful tool that provides fast and efficient topology optimized structures. This paper offers insight on the intricacies of unmanned aerial vehicle (UAV) design and discusses the various complications and advantages of using various drone geometries, manufacturing techniques, and materials. The interdependencies between geometry, manufacturing method, and material are also discussed. As such, the optimal frame type, manufacturing method, and material for optimized drone frame designs was found to be square-type, 3D-printing (MEX/FFF), and PEEK respectively. A generatively designed drone frame was created in Fusion 360 and analyzed using its own finite element analysis (FEA) capabilities; later, physical prototyping and testing verified the results gathered from FEA. This study attempts to re-introduce the feasibility and applicability of generative design in a sophisticated manner with the intention of closing gaps in novel research of drone frame optimization.

## Table of Contents

Abstract.....	2
List of Figures.....	3
List of Tables.....	5
Nomenclature.....	6
1.0 Introduction.....	7
1.1 Generative Design Principle.....	7
1.2 Mission and Purpose.....	8
2.0 Scope and Methodology of Study.....	8
2.1 Study Process Engine.....	9
2.2 Breakdown of Aspects.....	10
2.2.1 Geometry.....	10
2.2.2 Manufacturability.....	11
2.2.3 Material.....	12
3.0 Literature Review.....	13
3.1 Optimization of a quadcopter frame using generative design.....	13
3.2 A hybrid low altitude self-sustainable surveillance drone technology frame.....	16
3.3 A novel drone design using an optimization software.....	18
4.0 Theory and Trade Study.....	21
4.1 Geometry.....	21
4.2 Manufacturability.....	30
4.3 Material.....	40
5.0 Design Process.....	47
5.1 General Design Considerations.....	47
5.2 Preliminary Load Calculations.....	49
5.3 Generative Design Outcomes.....	52
5.3.1 Previous Iterations.....	53
5.3.2 Settings and Parameters.....	55
5.3.3 Analysis.....	59
6.0 Physical Design.....	64
6.1 Observations.....	64
6.2 Manufacturing Settings.....	66
6.3 Testing and Results.....	67
7.0 Conclusion.....	70
References.....	71
Appendix A.....	74
Appendix B.....	78
Appendix C.....	81

## List of Figures

Figure 1: Generative design inputs (left) and output (right). .....	8
---	---

Figure 2: Underlying pillars (aspects) of the design solution and optimized solution.....	9
Figure 3: Design of Experiments (DOE) engine [1]. .....	10
Figure 4: Means of analysis for geometry optimization. ....	11
Figure 5: Means of analysis for manufacturability optimization. ....	12
Figure 6: Means of analysis for material optimization. ....	13
Figure 7: Render of DJI flame wheel F450 drone frame [3].....	14
Figure 8: Generatively designed optimal design outcomes 1 (left) and 2 (right) [4]. .....	14
Figure 9: Major components of custom UAV [5]. .....	16
Figure 10: Custom drone frames depictions; from left to right: designs 1 to 4 [5]. .....	17
Figure 11: Frequency variation for increasing modal numbers [5]. .....	18
Figure 12: Original design of the drone using 3DEXPERIENCE [6]. ....	19
Figure 13: Drone parts: (a) centre top cover; (b) side top cover; (c) middle cover; and (d) arm [6]. .....	19
Figure 14: Hardware of drone design [6]. .....	21
Figure 15: Forces experienced by UAV during horizontal-translation steady-level flight shown from a side view. ....	22
Figure 16: Cantilever beam representation of drone arm.....	23
Figure 17: Arbitrary cross-section parameters for parallel axis theorem.....	24
Figure 18: Slight deformation caused by force distribution of drone. ....	25
Figure 19: Loads experienced by particles in the interface of arm and centre.....	26
Figure 20: Various types of drone frame types shown from the top view. ....	27
Figure 21: Attribute ranking for body type. ....	30
Figure 22: Compression molding process [10]. .....	31
Figure 23: Injection molding process [13]. .....	32
Figure 24: Typical 3D printing process [16]. .....	33
Figure 25: FFF/MEX 3D printing technology [18]. ....	34
Figure 26: Occurrences of (a) weld lines, and (b) delamination [16]. ....	35
Figure 27: Occurrences of defects in 3D printed parts: (a) layer separation and splitting; and (b) gaps between infill and outline [20]. .....	35
Figure 28: Attribute ranking for manufacturing methods. ....	40
Figure 29: Pyramid of polymeric materials in terms of availability, amorphous/semi-crystalline, and performance [22]. .....	42
Figure 30: Amorphous versus semi-crystalline material molecular chain structure [24]. ....	43
Figure 31: Attribute ranking for materials. ....	46
Figure 32: Pull-up maneuver (a) process, and (b) process with calculated loads. ....	49
Figure 33: Render of generative design outcome 1. ....	53
Figure 34: Generative design iterations showing preserve (green), obstacle (red), and starting (yellow) geometries. ....	54
Figure 35: Generative design outcomes 1, 3, 5, and 7 (left to right). .....	55
Figure 36: Obstacle and preserve geometries of the fifth iteration. ....	56
Figure 37: Engineering drawing of outcome 1 showing overall dimensions (mm). .....	58
Figure 38: Mesh parameters for generative design outcome 1. ....	59
Figure 39: Localized region of extremely low minimum factor of safety for load case 2. ....	63
Figure 40: Localized region of extremely high Von Mises stress for load case 2. ....	63
Figure 41: Localized region of extremely high displacement values for load case 2. ....	64
Figure 42: 3D printed generatively designed outcome 1. ....	65

Figure 43: 3D printing the drone body on the ORIGINAL PRUSA i3.....	66
Figure 44: Preview of 3D print on the ORIGINAL PRUSA i3 printer on Ultimaker Cura 5.1.0.....	67
Figure 45: Observed failure mode of load case 2. ....	69
Figure 57: Load case 1 final reading.....	78
Figure 58: Load case 2 final reading (brought to failure). ....	78
Figure 59: Load cases 3 and 4 final reading. ....	79
Figure 60: Prototype and waste material mass.....	80
Figure 61: Prototype mass after post-processing. ....	81

## List of Tables

Table 1: List of acronyms and abbreviations. ....	6
Table 2: Comparison of generative design frames with DJI F450 drone frame [4].....	15
Table 19: Physical properties of carbon fibre and ABS plastic [5].....	17
Table 21: Material properties discussed in [6].....	20
Table 3: Ranking criteria used for geometry selection. ....	28
Table 4: Advantages, disadvantages, and suitable materials of various manufacturing methods.....	36
Table 5: Ranking criteria used for manufacturing method selection. ....	38
Table 6: Material classification; adapted from [22]. ....	41
Table 7: Advantages and disadvantages of amorphous and semi-crystalline polymers [23].....	43
Table 8: Ranking criteria used for material selection. ....	44
Table 9: Decisions made for the conceptual design and reasonings for each decision. ....	47
Table 10: Pull-out maneuver phases, descriptions of phases, and assumptions made.....	50
Table 11: Pull-out maneuver phase and result per phase. ....	51
Table 12: Load cases applied as settings for generative design computation. ....	56
Table 13: Results from FEA analysis. ....	59
Table 14: Factor of safety contour maps for the four load cases. ....	60
Table 15: Von Mises stress contour maps for the four load cases. ....	61
Table 16: Total displacement contour maps for the four load cases.....	62
Table 17: Testing rigs corresponding to the load cases. ....	67
Table 18: Load case results. ....	68
Table 22: Method for determining frame attribute weights according to [9].....	74
Table 23: Frame type ranking using weights found by using method in [9]. ....	74
Table 24: Method for determining manufacturing-method attribute weights according to [9]. ....	75
Table 25: Manufacturing type ranking using weights found by using method in [9]. ....	75
Table 26: Method for determining material-property attribute weights according to [9]. ....	76
Table 27: Material properties of candidate materials [29]. ....	76
Table 28: Z-transformation and performance index values. ....	77

## Nomenclature

*Table 1: List of acronyms and abbreviations.*

<b>Acronym/Abbreviation</b>	<b>Definition</b>
<b>UAV</b>	Unmanned aerial vehicle
<b>AI</b>	Artificial intelligence
<b>MEX</b>	Material extrusion
<b>FFF</b>	Fused filament fabrication
<b>VTOL</b>	Vertical takeoff and landing
<b>DoE</b>	Design of experiments
<b>FEA</b>	Finite element analysis
<b>BMC</b>	Bulk molding compound
<b>SMC</b>	Sheet molding compound
<b>CAD</b>	Computer aided design
<b>CNC</b>	Computerized Numerical Control
<b>UTS</b>	Ultimate Tensile Strength
<b>YTS</b>	Yield Tensile Strength
<b>TMU</b>	Toronto Metropolitan University
<b>FRAMES</b>	Facility for Research on Aerospace Materials and Engineered Structures

## 1.0 Introduction

A recent surge in the popularity of drones enables the need for research in drones and related unmanned aerial vehicles (UAVs). Their practicality in various applications (such as in transportation, photography and videography, and conventional usage) while maintaining relatively low manufacturing/operating costs have made them popular amongst hobbyists, entrepreneurs, and businesses. An interesting and relevant area of study is on drone frame design since it entails the possibility for structure optimization (reducing weight and maintaining strength). Advancements in artificial intelligence (AI) have allowed structure optimization via generative design.

Generative design is a powerful iteration-based computational tool that has proven its practicality as a means of design for structures. It can be used to optimize the structural and thermal performance of structures by maintaining certain structural characteristics (e.g., rigidity, flexibility, and hardness) whilst reducing the overall mass of the structure. Increasing the performance of drone structures without increasing the mass is important in applications whereby vertical flight must be enabled (since upwards thrust must counteract the force of gravity).

Nevertheless, generatively designed components may be difficult to manufacture due to the complex nature of the outcome geometries; using high performance materials, in addition, may be difficult to shape using certain manufacturing methods. This study aims to explore the feasibility of generative design as a means of designing advanced aerial drone frames. The study is mostly concerned with the impositions generative design has on various manufacturing methods (mainly MEX/FFF printing) due to the complex nature of the organic shapes generated from generative design. Nonetheless, implications of geometrics and material choice on manufacturability are also explored. It should be noted that unmanned vertical takeoff and landing (VTOL) drones are the focus of this study.

### 1.1 Generative Design Principle

Generative design is a computational means of structural design that takes into consideration the following desired input parameters:

- Material
- Manufacturing method
- Geometries for preservation
- Obstacle geometries
- Structural Constraints
- Structural Loads
- Mass/rigidity objectives

The outcome of generative design is an organic structural network between preserve geometries (avoiding obstacle geometries) that best supports the force flow created from load and constraint definitions imposed on the software. The following schematic demonstrates this process:

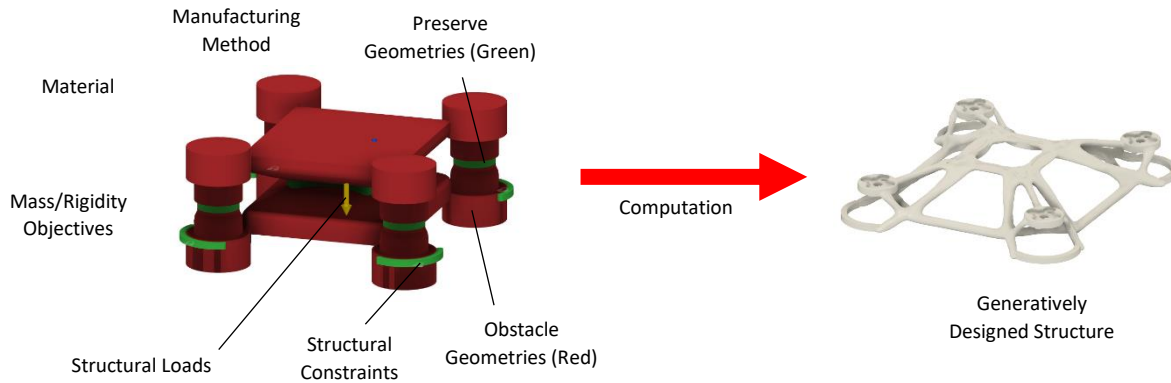


*Figure 1: Generative design inputs (left) and output (right).*

Generative design works by exploring many permutations of design through the development of infinitesimally small design elements to generate a solution to the inputs provided. Computational algorithms and artificial intelligence (AI) programs allow this process of exploration to be done quickly and effectively, ultimately providing many forms of optimized topological concepts upon which a designer may select and build.

## 1.2 Mission and Purpose

The underlying mission is defined as acquiring a lightweight and impact-resistant design solution for a 3D-printed drone body via generative design by the Fusion 360 software. This study aims to evaluate frame design, material selection, and 3D-printing fabrication methods via mathematical and experimental analysis of the drone body throughout the design process.

## 2.0 Scope and Methodology of Study

The scope of the study fits within the design and production of one quadcopter body. The study's scope is limited; through literature review, trade-off investigation, and load calculations, a generatively designed drone body may be created.

The mode of design throughout this report is the Design of Experiments (DoE) methodology. As such, the number of required trials to select the optimum 3D printing process parameters for the new drone design was reduced. Sub-elements and prototypes for testing were 3D printed at the Facility for Research on Aerospace Materials and Engineered Structures (FRAMES) at Toronto Metropolitan University (formally Ryerson University).

## 2.1 Study Process Engine

The design solution was developed with a firm understanding of the interrelationships between engineering aspects relative to the design scope. After careful consideration, it was decided that three aspects form the basis of the specific design solution. These three principal aspects are explored independently. Since they are interdependent, the interfaces between the three aspects were also explored. The three aspects dictating the design solution are its geometry, manufacturability, and material.

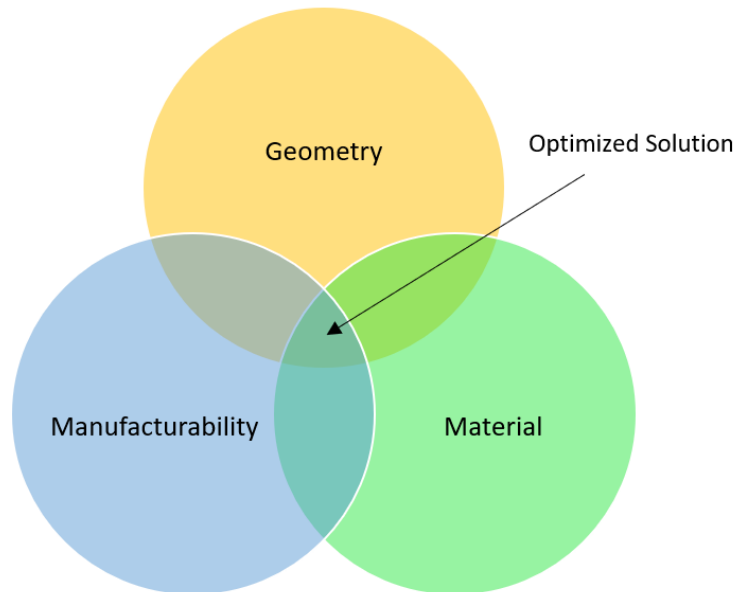


*Figure 2: Underlying pillars (aspects) of the design solution and optimized solution.*

The final design solution was a product of the Design of Experiments (DoE) engineering design process which exercises knowledge acquired from the independent and interdependent study between the three aspects within the scope of this design. The DoE forms the overarching design process within the scope. Investigation and verification of interdependencies of the three aspects aim to provide an optimized product through a cyclical process. The following diagram depicts the general workings of the DoE engine:

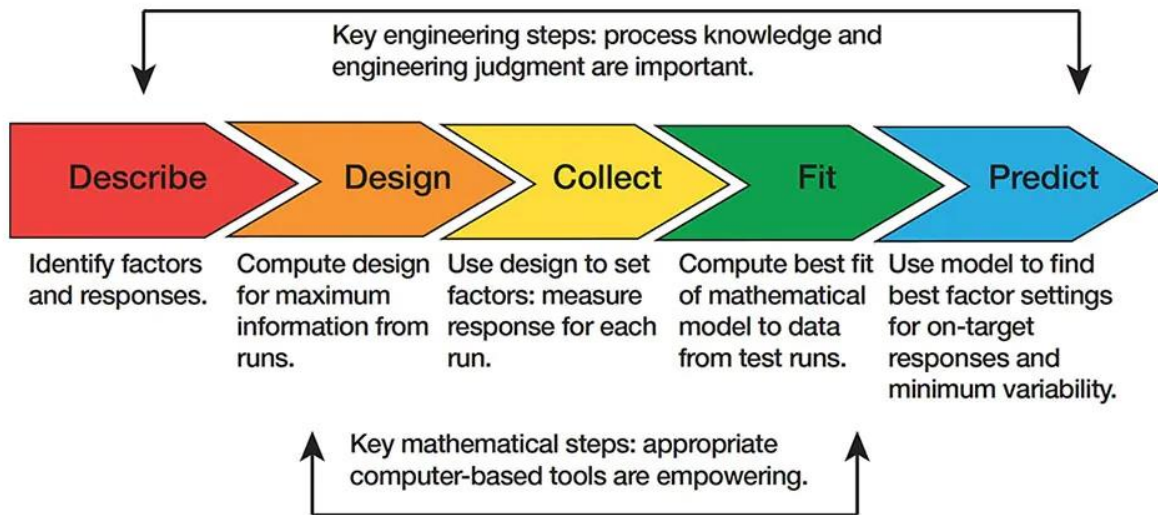


Figure 3: Design of Experiments (DOE) engine [1].

## 2.2 Breakdown of Aspects

As was mentioned in Section 2.1, the current study organizes the design problem into three distinct aspects; namely: geometry, manufacturability, and material. These three aspects were explored separately from one another. As such, each contains its implications for the design solution; each limits the design solution by providing design constraints. This section offers insight into the specific areas of interest corresponding to each aspect as well as the considerations that must be made when exploring each.

### 2.2.1 Geometry

The geometry of the aerial drone shall be designed to achieve rigidity and a higher impact-resistance-to-weight ratio. The following diagram demonstrates the means of geometry analysis:

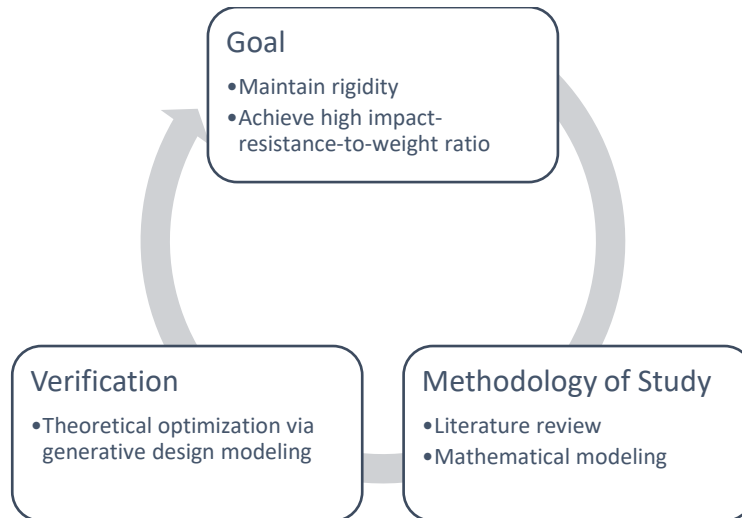


*Figure 4: Means of analysis for geometry optimization.*

### 2.2.2 Manufacturability

The manufacturing method for a high-performance aerial drone's frame is also within the scope of this study. Various manufacturing methods that have been used to manufacture drones in the past shall be explored; namely:

- Compression molding
- Injection molding
- 3D printing

The study of manufacturability entails considerations that must be made on the geometry and material. For example, different materials are used for different manufacturing methods. In addition, it is necessary to study the manufacturing constraints due to their influence on the geometry and material. The primary means of manufacturing to be explored in this report is material extrusion (MEX), also called fused filament fabrication (FFF) which is a 3D printing technique. Manufacturing constraints depend on the specific machine used to fabricate the model, its build specifications (e.g., build volume), and tolerances.

Certain parameters must be considered when considering the MEX/FFF manufacturing technique:

- Type of printer
- Model of printer
- 3D printing tolerances
- Thinnest walls possible
- Minimum turning radius
- Nozzle and bed temperature

Printer capability testing shall be conducted before investigation when using MEX/FFF fabrication methods and is explored in Appendix A. The following diagram demonstrates the means of manufacturability analysis:

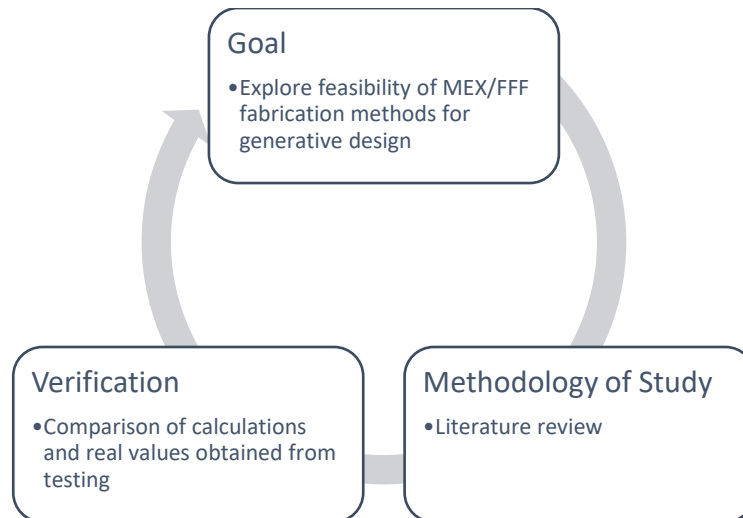


*Figure 5: Means of analysis for manufacturability optimization.*

### 2.2.3 Material

Material selection is important in defining the overall structure and dictates the drone's capabilities in flight. Material shall be selected to achieve rigidity and a higher impact-resistance-to-weight ratio. The following summarizes the possible materials to be used within the scope of this study:

- Pure polymers
  - Low-temperature polymers
  - High-temperature, high-performance polymers
- Polymers reinforced with discontinuous fibres
  - Low temperature
  - High temperature
- Polymers reinforced with continuous fibres
  - Low temperature
  - High temperature

Composite materials consisting of a polymeric matrix and reinforcement significantly improve the performance of a material. For the case of drone body study, it is necessary to use a material that ensures acoustic stability and rigidity while being lightweight. The following diagram demonstrates the means of material analysis:

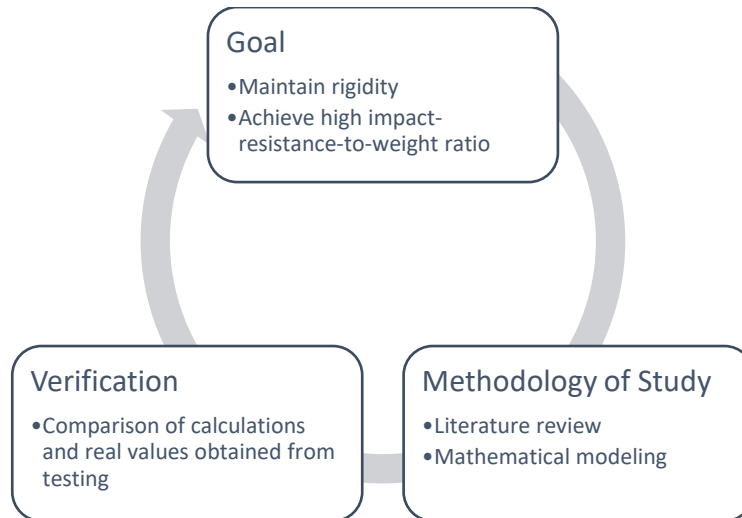


*Figure 6: Means of analysis for material optimization.*

### 3.0 Literature Review

Though the implementation of generative design is the main focus of the study, it was important to establish a basic understanding of shortcomings from previous drone designs. 3D printing specifically has allowed for a surge in interest in drones amongst amateurs. Moreover, after Amazon announced it would use drones for delivery in 2013 [2], drones' applicability in commercial industries has become more evident. Documentations for both the design and manufacturing of unmanned aerial vehicles provide insightful information regarding materials used and the shortcomings of said material selection and componential design. This literature review aims to explore:

- Previous UAV designs (including geometry, method of manufacturing, and material)
- The shortcomings of the previous designs
- Potential takeaways that may be implemented in the current study

The literature review presented in this study is not limited to generatively designed UAV frames. The literature review aims to provide a better understanding of geometry, manufacturability, and material, and their implications on the design solution.

#### 3.1 Optimization of a quadcopter frame using generative design

In the study presented by Bright et al [4] in 2021, the implications of designing a drone frame using generative design tools were explored. Autodesk generative design embedded in Fusion 360 was used to compare two generatively designed drone frames with the traditional DJI flame wheel F450 drone frame. The study demonstrated minimum displacement in the generatively designed body compared to that of the traditional drone frame. Finite element analysis (FEA) conducted

through Fusion 360’s built-in software was used to simulate internal body stresses resulting from external loads on the frame. Static stress-strain, modal frequency, and displacement were the parameters that were explored and compared between the traditional body and the two generatively designed solutions. Figure 7 shows the traditional DJI F450 drone frame:



*Figure 7: Render of DJI flame wheel F450 drone frame [3].*

The DJI flame wheel F450 drone frame is an example of a “true-X” type frame. Other quadcopter (characterized as having four rotors) frames include the “hybrid-X”, “stretched-X”, “square”, and “H” type frames. The iterative design exploration process computed numerous design options—74 designs—two of which were taken to be later compared to the traditional drone frame [4]. The two design outcomes were considered to be the most suitable and pertinent based on the study’s design requirements. The selection was done by considering stress-strain relations, behavior to vibration, the total weight of the frame, and the minimum factor of safety. The two generatively designed solutions can be seen in Figure 8.



*Figure 8: Generatively designed optimal design outcomes 1 (left) and 2 (right) [4].*

Table 2 lists the properties obtained through Fusion 360’s generative design capabilities. It should be noted that the designs were generated according to the flight envelope of the traditional drone.

In other words, the load cases that the traditional frame would experience in flight were applied in the settings of the generatively designed outcomes. The control variables between all frames of this study included (1) the weight of each component needed to be carried on the drone during flight, and (2) the overarching size of the drone [4]. Table 2 is a summary of the results obtained in the study.

*Table 2: Comparison of generative design frames with DJI F450 drone frame [4].*

<b>Factors</b>	<b>Frame 1</b>	<b>Frame 2</b>	<b>DJI F450 frame</b>
<b>Weight of the frame (g)</b>	227	267	330
<b>Minimum factor of safety</b>	13.3	133	3.301
<b>Manufacturing method</b>	Additive manufacturing	Additive manufacturing	Advanced manufacturing
<b>Maximum von Mises stress (MPa)</b>	1.5	17.11	21.33
<b>Maximum displacement global (mm)</b>	6.22	0.01	4.016
<b>Material used</b>	ABS plastic	ABS plastic	Polyamide nylon
<b>Filament spent (length)</b>	0.7 m	0.21 m	Not available

It should be noted that acrylonitrile butadiene styrene (ABS) was chosen due to its high rigidity, impact resistance, and tensile strength [4]. Specific settings in generating the bodies as well as other outcomes such as estimated cost and volume in this study may be explored in [4]. Overarching CAD designs, obstacle and preserved boundaries, factor of safety limits, and load cases may also be explored in [4]. Three notable improvements in performance from the generatively designed frames compared to the traditional frame were elucidated in the study. Designing via generative design demonstrated the potential for (1) significant increases in factor of safety, (2) significant increases in yield/fracture resistance shown by lower von Mises stress, and (3) significant increases in deformation resistance—all whilst enabling the reduction of weight [4]. The comparisons for stress-strain, displacement, and modular frequency between the three frames of two different materials were provided as well.

The study specifically addressed a true-X type quadcopter frame fabricated through additive manufacturing with ABS plastic. Not only did the generative designed frame demonstrate minimum displacement compared to traditional designed drone frame, it also yielded greater resistance to fracture. Considering the information obtained in [4], the current study may explore the relationship between multiple iterations of generative design for the factor of safety, yield/fracture resistance, and deformation resistance. ABS plastic was proven to be a candidate material for the manufacturing of a generatively designed quadcopter frame.

### 3.2 A hybrid low altitude self-sustainable surveillance drone technology frame

S. Sundararaj et al [5], using commercially available simulation software, explored structural and modal comparisons of different versions of a custom type of drone frame using carbon fibre and acrylonitrile butadiene styrene (ABS) materials. The drone's propulsive system consists of three rotors underneath a lighter-than-air gas chamber with an array of solar cells to power the rotors. The following diagram depicts the major components of the UAV presented in the study:

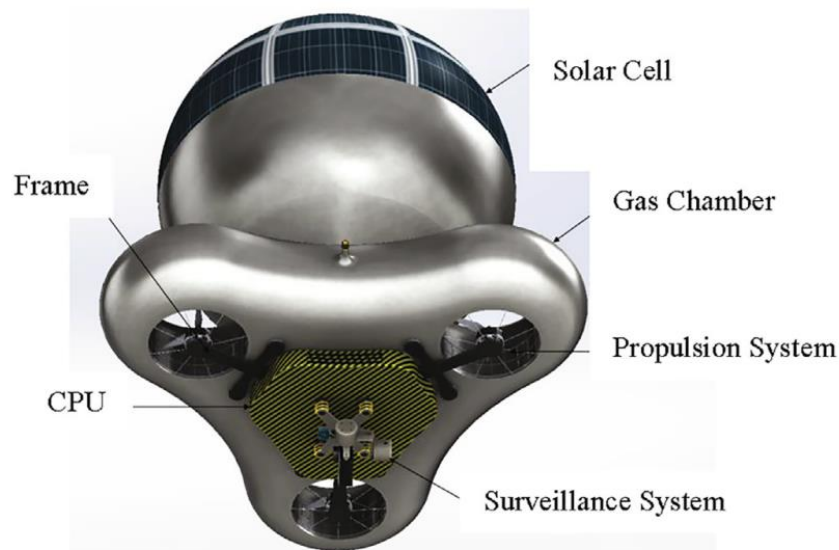


*Figure 9: Major components of custom UAV [5].*

Four versions of the frame were explored in the making of the study's self-power-sustaining drone: (1) directly connected triangular frame, (2) short-armed semi-circular frame, (3) long-armed semi-circular frame, and (4) short-armed rectangular frame. The parameters that were used to compare the performance of each structure and material included maximum permissible stress, strain displacement, and frequency values. Compared to the other two versions, the connected triangular frame (1) and long-armed semi-circular frame (3) demonstrated less strength but greater manufacturability [5]. The short-armed semi-circular frame (2) and short-armed rectangular frame (4) were complex to manufacture but they showed high strength to withstand the induced stress [5]. Figure 10 shows all four designs:

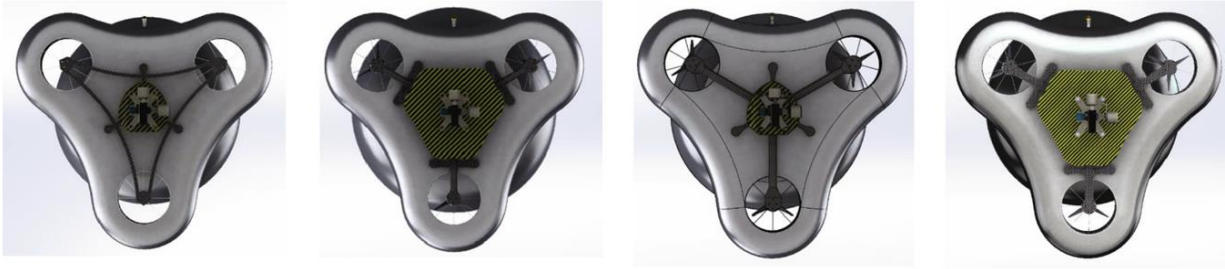


Figure 10: Custom drone frames depictions; from left to right: designs 1 to 4 [5].

The frames were designed with consideration of the mounted components that would be supported by the frame. Because the UAV's objective was to achieve longer flight durations, it was necessary to explore possibilities for lightweight and strong frames [5]. In all cases of FEA analysis (stress-strain, displacement, and frequency), a total load of three newtons was applied [5]. Von Mises stress, equivalent strain, and displacement contours on each analysis were generated and discussed.

Von Mises stresses were maximum in Version 1 and Version 4; the locations of these high values are characterized by connection points between the arms and the central part of the frame. Version 2 and Version 3 demonstrated less induced stress compared to the other two versions. The study suggests that carbon fibre is a suitable choice for drone frames since, when compared to the harder ABS plastic, carbon fibre demonstrated lower centralized stresses [5].

Equivalent strain contours obtained from simulation demonstrated maximum strain values in Version 2 and Version 3. In all cases, it was found that the joint sections between the arms and the central part of the frame experienced the greatest strains; this phenomenon corresponds to the high von Mises stresses at these same locations. In all cases, the greatest strains were observed at the end of each arm where they connect with the rotors. Greater displacements were found in carbon fibre than in ABS plastic due to the higher brittleness of ABS plastic.

Table 3: Physical properties of carbon fibre and ABS plastic [5].

Physical Property	Carbon Fibre	ABS Plastic
Elastic Modulus (N/m <sup>2</sup> )	7E10	2E9
Poisson's Ratio (No unit)	0.23	0.394
Shear Modulus (N/m <sup>2</sup> )	5E9	3.189E8
Mass density (kg/m <sup>3</sup> )	1550	1020
Tensile Strength (N/m <sup>2</sup> )	6E8	3E7
Compressive Strength (N/m <sup>2</sup> )	5.7E8	6.5E7
Yield Strength (N/m <sup>2</sup> )	2.23E11	4.35E7

Modal vibration analysis was done by exploring simulations demonstrating the forces within the bodies undergoing various frequencies of vibration. As such, natural frequencies of the frame geometries and materials were explored. Figure 11 depicts frequencies per modal number of each material and geometry couple.

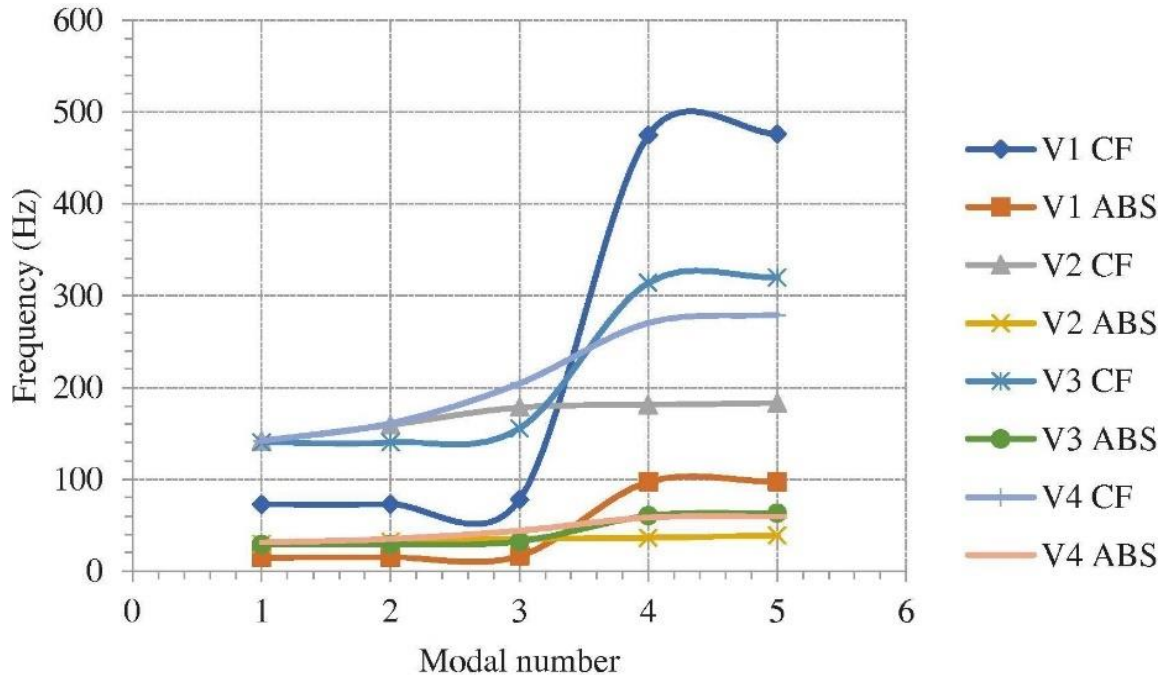


Figure 11: Frequency variation for increasing modal numbers [5].

Due to ABS plastic's higher brittle properties, the natural frequencies of ABS plastic bodies were lower than those of carbon fibre. In addition, due to lesser cross sections and longer lengths, frames with longer arms were found to show lower natural frequencies. Version 1 and Version 3 show higher susceptibility to failure due to their longer arms.

The results demonstrated in [5] prove the success of specific geometry characteristics for generating strong and lightweight drone bodies. Considerations for obtaining an optimized drone body include (1) designing the frame with shorter arms more integrated with the central part of the frame if the main concern is vibration failure, (2) designing the frame with as least sharp corners (where intersections occur) as possible, and (3) designing the frame to obtain an optimized balance of rigidity and strength to reduce instability and the possibility of fracture.

### 3.3 A novel drone design using an optimization software

The research work by MohamedZain et al. [6] presents the design and design process of a small-sized UAV using the 3DEXPERIENCE software. The design process began with the selection of materials; namely polylactic acid (PLA), acrylonitrile styrene acrylate (ASA), and acrylonitrile butadiene styrene (ABS) were selected and studied. The overall outlook of the design may be

explored in Figure 12. Four main parts make up the body of the drone: the centre top cover, the side top cover, the middle cover, and the arms. These four parts are presented in Figure 13. Using the analytical software, a trade-off study was presented to finalize the geometry of each part as well as the settings involved in software design catering to the individual needs of each part.

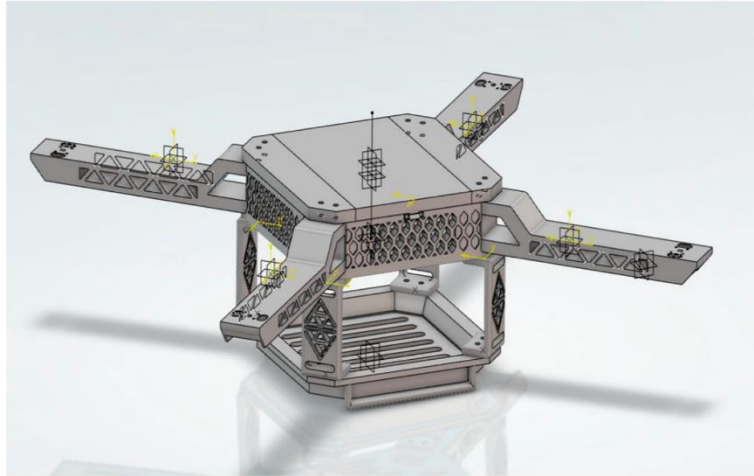


Figure 12: Original design of the drone using 3DEXPERIENCE [6].

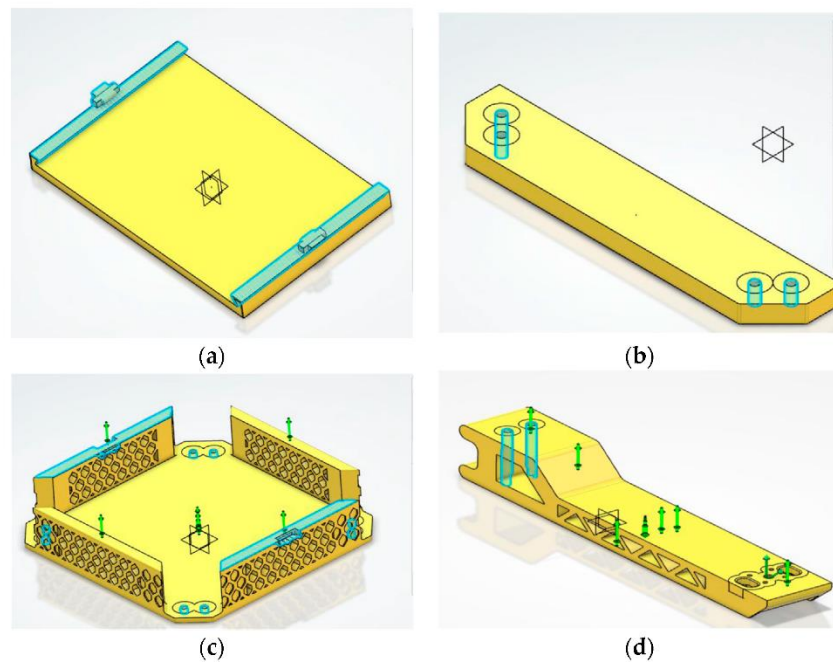


Figure 13: Drone parts: (a) centre top cover; (b) side top cover; (c) middle cover; and (d) arm [6].

The report discusses the possibility of using different drone body shapes. The study discusses the differences between the X-design, H-design, and hybrid H-design. The X-design is characterized

by being lightweight and nimble [7] and also provides the most stability in flight due to its geometrical symmetry [6]. Moreover, the X-design chassis is easy to control and maneuver and, in addition, hovers longer compared to the other chassis [6].

To simulate and manufacture a prototype, additive manufacturing was chosen as the manufacturing method—specifically fused filament fabrication (FFF) was selected. Specific loads were theoretically established based on the loads that the drone would experience during launching and landing. The design of the drone is consistent in the use of honeycomb structures since they reduce the weight of the drone and increase the structural impact resistance [6]. Moreover, it allows for heat dissipation and cooling for the electrical components which in turn increases their lifespans. According to MohamedZain et al. [6], the “hexagonal shape of the honeycomb design is usually the strongest shape”. The material candidates chosen for analysis were PLA, ASA, and ABS materials. The research values the incorporation of some degree of flexibility of the arms. PLA was chosen for the parts that required high density, stiffness, and strength—it was selected for the inner part of the drone. ABS was chosen over ASA for some parts of the drone due to its higher stiffness and strength. ABS was chosen to replace PLA in some locations since it is more lightweight. It was also chosen since it fulfilled the requirements and budget constraints. Nevertheless, for the sake of simulation, only the core material was explored.

*Table 4: Material properties discussed in [6].*

<b>Material</b>	<b>PLA</b>	<b>ASA</b>	<b>ABS</b>	<b>PETG</b>
<b>Density (kg/m<sup>3</sup>)</b>	1240	1070	1050	1270
<b>Young’s Modulus (MPa)</b>	1.98E9	1.35E9	1.70E9	1.38E9
<b>Poisson Ratio</b>	0.33	0.33	0.33	0.33
<b>Maximum Stress before breaking (MPa)</b>	47	28	35	-

After material and geometrical considerations were discussed, the drone design stress and strain simulation were executed and analyzed. The design was also 3D printed via FFF using an ANYCUBIC I3 MEGA printer to actualize the design. Figure 14 shows the fabricated drone.



*Figure 14: Hardware of drone design [6].*

This study demonstrated extensive knowledge of the type of body selected for the drone and its implication for the structural performance of the drone in flight. It was also helpful in acquiring a greater understanding of material candidates and the characteristics dictating the success of the drone frame.

## 4.0 Theory and Trade Study

This section discusses the three aspects of a successful drone design: (1) geometry, (2) manufacturability, and (3) material, as well as a combination of these three aspects in various iterations for the overall design. These topics are crucial to be considered in the design of a lightweight yet strong drone body. Using a newly established understanding of these topics obtained from literature review considerations, it was possible to discuss the three aspects independently from one another as well as the implications that each may have on the other. Hence, this topic is concerned with discussing the trade-offs of using different drone body geometries, manufacturing methods, and materials.

### 4.1 Geometry

The geometry of drone frame design is a factor that is crucial in increasing the strength-to-weight ratio since it is directly correlated with the flow of force imposed on the structure by force-generating conditions that UAVs must undergo. In general, the forces experienced by a drone in typical vertical and steady-level flight are lift, drag, weight, and thrust. Thrust and lift are equal

when no component of thrust generated by the propulsion system contributes to horizontal acceleration.

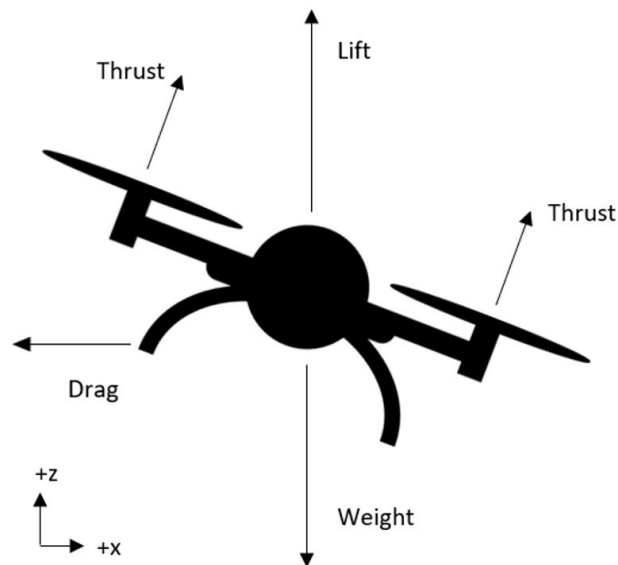


*Figure 15: Forces experienced by UAV during horizontal-translation steady-level flight shown from a side view.*

Figure 15 demonstrates the typical loads relevant to an x-z and y-z symmetrical UAV under horizontal steady-level flight. In this case, lift is a +z component of the thrust created by the propulsion system. The vertical component of thrust equates to the lift. The weight of the drone always faces the -z direction. Drag always faces opposite the direction of travel. Lift is equal to weight in steady-level flight. The typical force flow within the arm of the drone may be simplified to a cantilever beam experiencing a load at its end as follows:

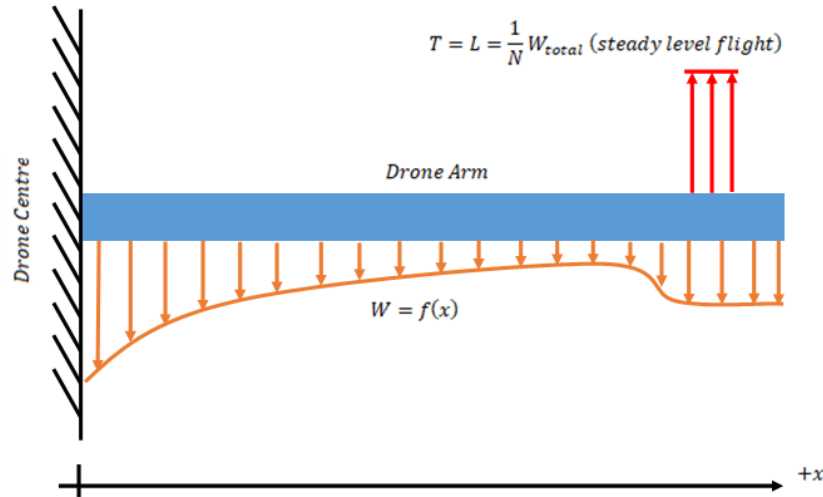


Figure 16: Cantilever beam representation of drone arm.

Figure 16 demonstrates a simplification for force analysis through a drone arm; cantilever beam analysis allows for a general understanding of the shear and moment forces acting through the beam at different locations. This analysis assumes that only forces in the z-plane are applied to each arm. In general, using the cantilever beam simplification shown in Figure 16, the drone is most likely to experience maximum shear and bending moment at the interface between the arm and the centre; maximum deflection is most likely to occur at the axis of propeller rotation. The equations represented in Figure 16 are as follows:

$$T = L = \frac{1}{N} W_{total} \text{ (steady level flight)} \quad (1)$$

$$W = f(x) \quad (2)$$

Equation 1 describes thrust as equal to lift (in the case of no horizontal translation and steady-level flight). Equation 1 also assumes that each arm carries an equal amount of the drone's total weight with "N" being the number of arms. Moreover, it is assumed that no torque is being applied around the arm's cross-sectional plane's neutral axis. Equation 2 describes the weight of one arm as a function of distance along the arm. The weight load may or may not be distributed evenly; this is dependent on the cross-sectional shape as well as the material chosen for the frame. The equations describing bending moment and shear loads are as follows:

$$\sigma_b = -\frac{My}{I} \quad (3)$$

$$\tau = \frac{VQ}{It} \quad (4)$$

In Equation 3,  $\sigma_b$  is the bending stress,  $M$  is the local moment, and  $I$  is the moment of inertia about the neutral axis. In Equation 4,  $\tau$  is the transverse shear stress,  $V$  is the local shear force,  $t$  is the local width at the point of shear stress,  $I$  is the moment of inertia about the neutral axis, and:

$$Q = A\bar{y} \quad (5)$$

In Equation 5,  $A$  is the area of the section above the point of shear stress and  $\bar{y}$  is the distance of the centroid of the area from the neutral axis. The moment of inertia is defined as the degree of resistance to angular acceleration and is related to any arbitrary cross-section by the parallel axis theorem:

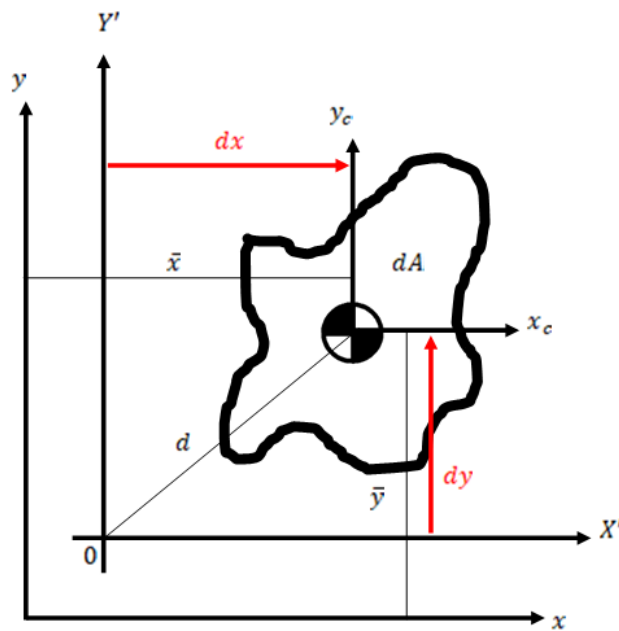


Figure 17: Arbitrary cross-section parameters for parallel axis theorem.

The parallel axis theorem states that the sum of the moment of inertia concerning the centroidal axis, and the product of the area and the square of the distance between the two axes, is the moment of inertia with respect to any given axis. For any arbitrary cross-section:

$$I_x = I_{x_c} + Ad_y^2 \quad (6)$$

$$I_y = I_{y_c} + Ad_x^2 \quad (7)$$

One of the strongest cross-sections in preventing shear failure as well as bending moment failure for a cantilever beam is that of the I-beam. Its flange can effectively withstand large bending stress and its web distributes shear along its face. Knowledge of these stress-distributing characteristics may aid in producing effective generative designs and also allows for discussion on the effectiveness of these designs.

Considering the overall body of the drone, Figure 16 suggests that deflection upwards deflection (+z) is inevitable, even in the case of steady-level flight since there is no equal localized downwards force counteracting the thrust of one propeller. This suggests that inward moments will be applied to the centre of the frame and the overall body of the drone will “sag” according to Figure 18.

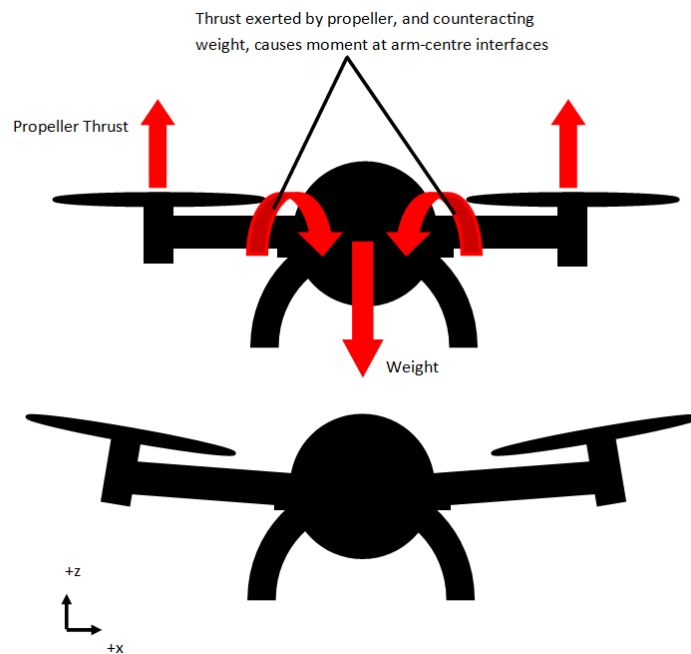


*Figure 18: Slight deformation caused by force distribution of drone.*

A particle located at the interface will undergo tension at its bottom and compression at its top (which is a positive bending moment). Shear will also be induced in those locations due to the adjacent particles next to it.

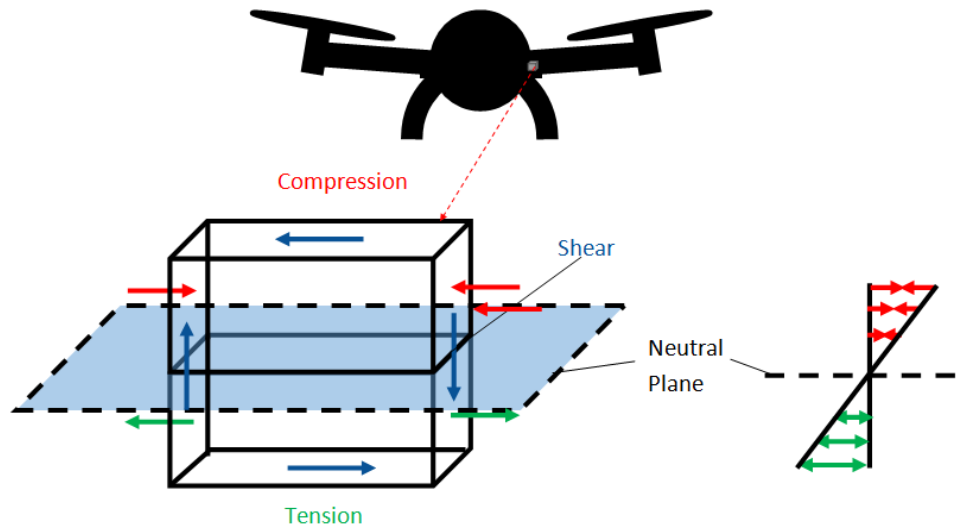


*Figure 19: Loads experienced by particles in the interface of arm and centre.*

The geometry of the drone components is one parameter that dictates the drone's resistance to failure due to induced stresses since it is the means of load distribution. The cross-section of the arm, for example, is a crucial consideration since it must distribute the loads accordingly. The all-embracing means of drone structure success in terms of geometry is the reduction of high-stress points via even load distribution. Of course, the entire purpose of generative design is to solve this otherwise complicated problem of generating the best load-distributing geometry. Exploring the loads on the particle and overall drone allows a general theoretical understanding of generative design outcomes:

- Having multiple “beams” connected from the centre body to arm
  - Increases connection points though it distributes the load better
- Including a wider-area network of connection points on the interface of arms and centre
  - Increases strength at the interface to support the maximum bending moment and shear
- Using specific non-constant cross-sectional geometries
  - Supports localized loads to provide sufficient resistance to bending moment and shear while reducing weight

Overall drone geometry has a significant effect on strength and stability. The question of which drone body type to use is directly correlated with the forces shown in Figure 15. There are several types of drone bodies (only drones with four rotors are considered):

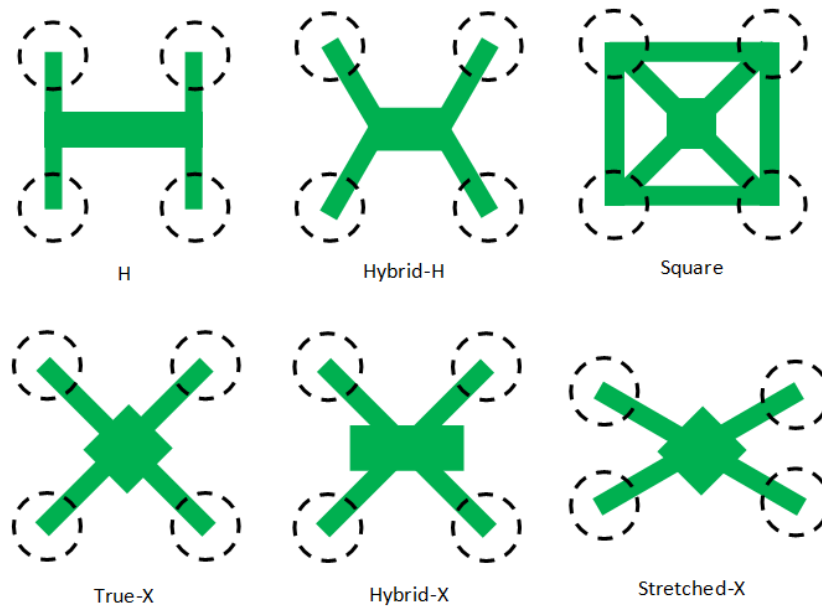


*Figure 20: Various types of drone frame types shown from the top view.*

Each type has distinct advantages and disadvantages, making it more suited to specific applications. Using force flow knowledge for investigating the intermolecular load distribution, predictions concerning body type's implications on load distribution across the frame may be generated. In a study done by J. Castiblanco et al. [7], the dynamic behaviour of drones designed for racing competitions is explored. This study found that the true-X design has the advantage of being light though it requires long landing gear. The true-X symmetrical airframe was found to provide a constant time frequency and speed rate during trajectories because its flight behaviour is reliable—indicative of high maneuverability and agility. Stretched-X models, due to their lightweight, reached the fastest speeds; however, they do not exhibit the same level of speed during curved trajectories [7]. This means that they are less maneuverable. According to Basson et al. [8], The true-X is the lightest frame and has torsional stiffness though it requires long landing gears when mounting sensory equipment which may counteract the lightweight frame. The H-frame is characterized by being heavy due to its large size. The H-frame may also experience problems with torsional stiffness though it is an appropriate body choice for front-mounted sensory equipment. In addition, minimal landing gear is required. The hybrid-H body type has advantages and disadvantages from both the H-frame and true-X design. Having a shorter body reduces torsional stress issues. The hybrid-H requires shorter arms than the true-X frame though longer arms than the H-frame. This may imply that shorter arms enable more stability than longer arms. The hybrid-H design, like the H-frame, is also suited for front-mounted sensory equipment and requires minimal landing gear.

Based on literature and knowledge of drone applications, a preliminary estimate for ranking the attributes of the various drone bodies was generated. Table 5 lists the criteria and criteria weightings by which Figure 21 was generated.

*Table 5: Ranking criteria used for geometry selection.*

<b>Criteria</b>	<b>Description</b>	<b>Weight (%)</b>
<b>Safety</b>	Safety describes both the ability to prevent, and mitigate, potential harm to the user and the flight environment induced by the drone (both in and out of operation). A higher degree of safety is desired.	13.9
<b>Stability</b>	Stability refers to the overall ability of the drone to act as commanded and the unlikelihood of the drone losing control. A higher degree of stability is desired.	12.2
<b>Maneuverability</b>	Maneuverability is defined as the ability of the drone to make quick and various motions in flight whilst maintaining its structural integrity. A higher degree of maneuverability is desired.	8.89
<b>Impact Resistance</b>	Impact resistance refers to the unlikelihood of the drone being totaled due to a collision. A higher degree of impact resistance is desired.	12.2
<b>Power-to-weight</b>	The power-to-weight ratio refers to the drone's ability to handle stress due to potential propulsive power whilst maintaining a lightweight body. A higher degree of power-to-weight is desired.	9.44
<b>Manufacturability</b>	Manufacturability describes the ability of the drone to be manufactured using conventional techniques. A higher degree of manufacturability is desired.	11.1
<b>Maintainability</b>	Maintainability refers to the ability of the drone to be consistently maintained; this section also encapsulates any aspect dictating the accessibility of components for repair and replacement. A higher degree of maintainability is desired.	9.44
<b>Complexity</b>	Complexity is defined as the overall user-friendless and ease of usage encapsulating both manufacturability and the overall look of the drone. This is directly correlated with manufacturability. A lower degree of complexity is desired.	7.22

<b>Cost-Effectiveness</b>	Cost-effectiveness refers to the ease of creating, manufacturing, assembling, and maintaining the drone body. A higher degree of cost-effectiveness is desired.	6.67
<b>Flight Efficiency</b>	Flight efficiency refers to the ability of the drone to consume low power and maintain its flight for long periods of normal operation.	8.89

Table 5 above defines all the attributes independent of any implications by any other subsystems, such as guidance, navigation, and control. The numerical weight assigned to each was assigned according to what was believed to hold the greatest accreditations for flight readiness according to the method described in [9]. Safety, for example, was given the greatest priority.

The overall geometry of the drone was selected based on the criteria and weightings described in Table 5. Figure 21 demonstrates the rankings of each body type according to Table 22 in Appendix A.

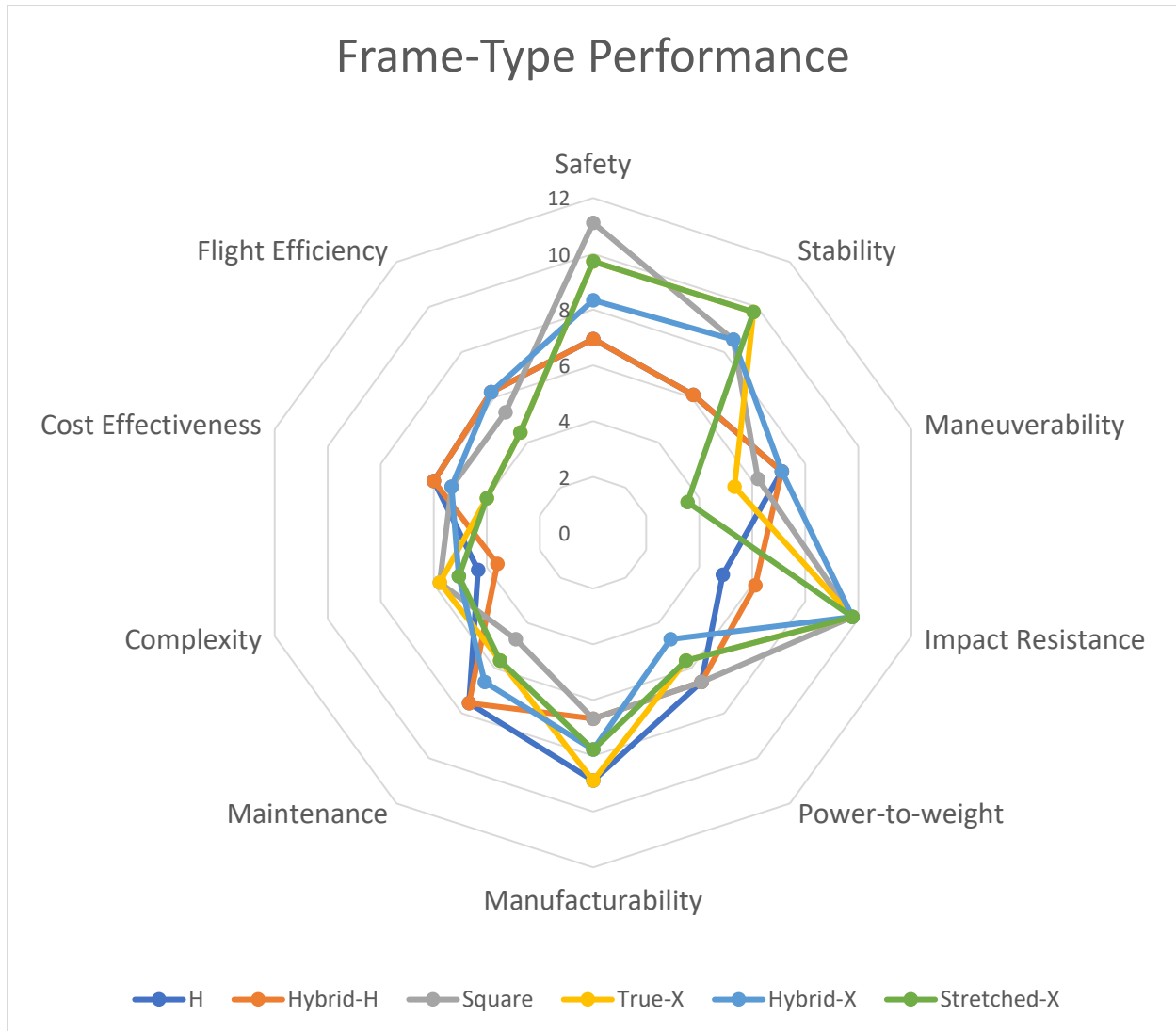


Figure 21: Attribute ranking for body type.

The rankings for each body type according to the criteria were given based on the information and knowledge obtained in this study. The numbers provided in Figure 21 are that of weighted percentiles; the addition of all percentiles for a given frame type gives an average score of less than 100%. The greatest score that was achieved was the square frame with a score of 70.4%. The second and third highest ranking bodies were hybrid-X and true-X respectively. It should be noted that Figure 21 simply attempts to visually compare the attributes for each body type presented.

## 4.2 Manufacturability

Manufacturability has a strong implication on the design of the UAV frame. The geometry, being important to the success of a drone frame, is directly correlated with its manufacturability. It is impractical to discuss the geometry of the UAV without discussing whether or not said geometry

can be created. Manufacturability also entails the number of parts that comprise the drone frame since a unibody frame may not be possible to manufacture for certain manufacturing techniques. The question of whether the drone should be unibody or have multiple parts is a crucial determinant of the frame's considerations in terms of manufacturability. The implications on manufacturability by the material choice are also vital considerations when choosing manufacturing methods. To theorize a quadcopter design with a high strength-to-weight ratio, it is necessary to explore manufacturability; different manufacturing methods are explored in this section:

- Compression Molding
- Injection Molding
- 3D printing (MEX/FFF)

Compression molding is the manufacturing method that is characterized by compressing material into a mold cavity whilst applying heat to cure the material. The raw materials for compression molding come as preforms, putty, or granules; the material is placed in an open, heated mold cavity where it is compressed. Overflow grooves allow excess material to flow out of the mold. After curing, the mold is opened, and the molded compound is removed [10]. Figure 22 depicts the process of compression molding.

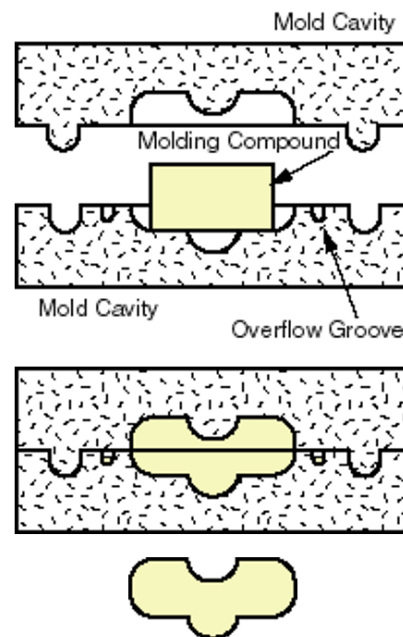


*Figure 22: Compression molding process [10].*

Compression molding is commonly used in manufacturing thermoset plastics such as epoxy, silicone, polyurethane, and phenolic, though it is also applicable to thermoplastics such as polyetheretherketone (PEEK), polyimide (PI), and fibre-reinforced plastics [10]. Compression molding is a viable option for manufacturing a unibody drone frame; it is also viable for

manufacturing parts that may later be assembled using connection methods. Bulk Molding Compound (BMC) and Sheet Molding Compound (SMC) are two types of compounds used in compression molding [10]. SMCs, although more expensive, can be pre-cut to conform to the surface area of the mold which may result in less flow orientation allowing for higher product consistency [10]. Compression molding is ideal for high-volume production, has low post-manufacturing challenges, is energy efficient, and produces minimal material waste though it is limited in creating complex geometrics and diameter closures that are greater than 48mm [11]. Compression molding is well suited for generating composite parts which offer high mechanical strength, dimensional stability, rigidity, and a high strength-to-weight ratio—moreover, increased electrical, moisture, and temperature resistances [12]. Table 6 summarizes the advantages and disadvantages of using compression molding as a manufacturing method.

Injection molding, similar to compression molding, also is characterized by having a mold though instead of having a “pressing” means of formation, molten products are solidified through cooling after being injected into the mold. Figure 23 shows the workings of an injection molding process.

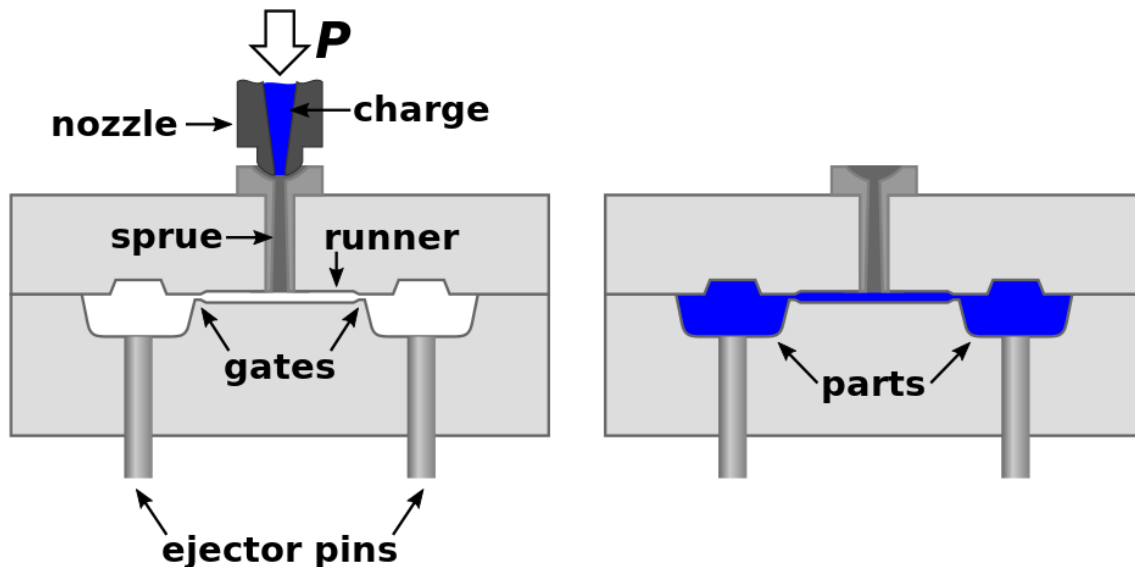


*Figure 23: Injection molding process [13].*

Injection molding process works only through the control of heat transfer and pressure flow; these two mechanisms significantly impact the final polymer-chain structure and hence, the performance of the structure. Degree of crystallinity for semicrystalline polymers, for example, is controlled by defined in-mold cooling rates [14]. Since injection molding does not depend on force distribution like compression molding, it is capable of producing more complex geometrics; the viscous material may flow to any void areas set by the mold [11]. Injection molding is ideal for

complex designs, multiple size runs, and offers flexibility in colour and material [11]. Moreover, injection molding is a suitable approach to manufacturing prototypes since it has shorter lead times [15].

Additive manufacturing, also called 3D printing, is a distinct form of manufacturing from compression and injection molding. Additive manufacturing fabricates 3D parts layer by layer. 3D printing was first used in the 1980s to develop prototype parts and it was previously referred to as “rapid prototyping” [16]. As the name implies, the strength of 3D printing is its ability to develop many complex shapes quickly and without the need to manufacture external creation tools such as molds. 3D printing is tied with computer-aided design (CAD) software which facilitates the creation of digital designs. 3D printing, like computerized numerical control (CNC) machines, is a means of physical realization from a digital design. 3D printing works by enabling x-plane, y-plane, and z-plane translation of a nozzle that deposits material onto a heated print bed. Depending on the material being printed, different parameters such as nozzle temperature, print-bed temperature, flow speed, filament diameter, and environmental attributes such as moisture must be specified. The following diagram depicts the general workings of 3D printing:

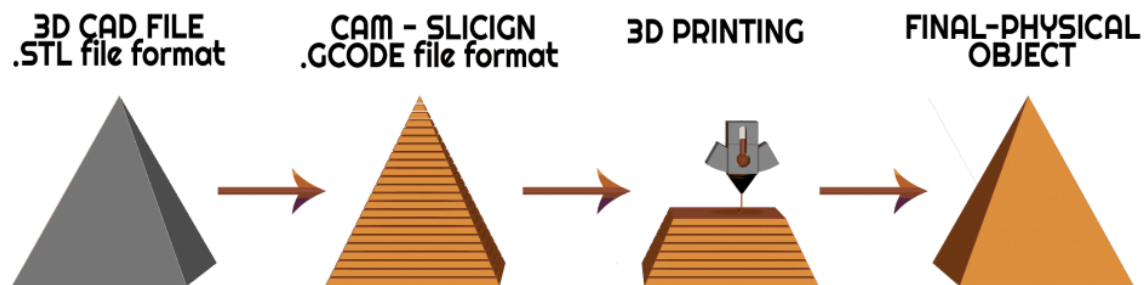


*Figure 24: Typical 3D printing process [16].*

Though the general working principle is the same, there are different types of 3D printing methods; in this study, specifically material extrusion (MEX), also called fused filament fabrication (FFF), are discussed. MEX 3D printing technology deposits molten material from a feedstock on a build platform to manufacture a part [18].

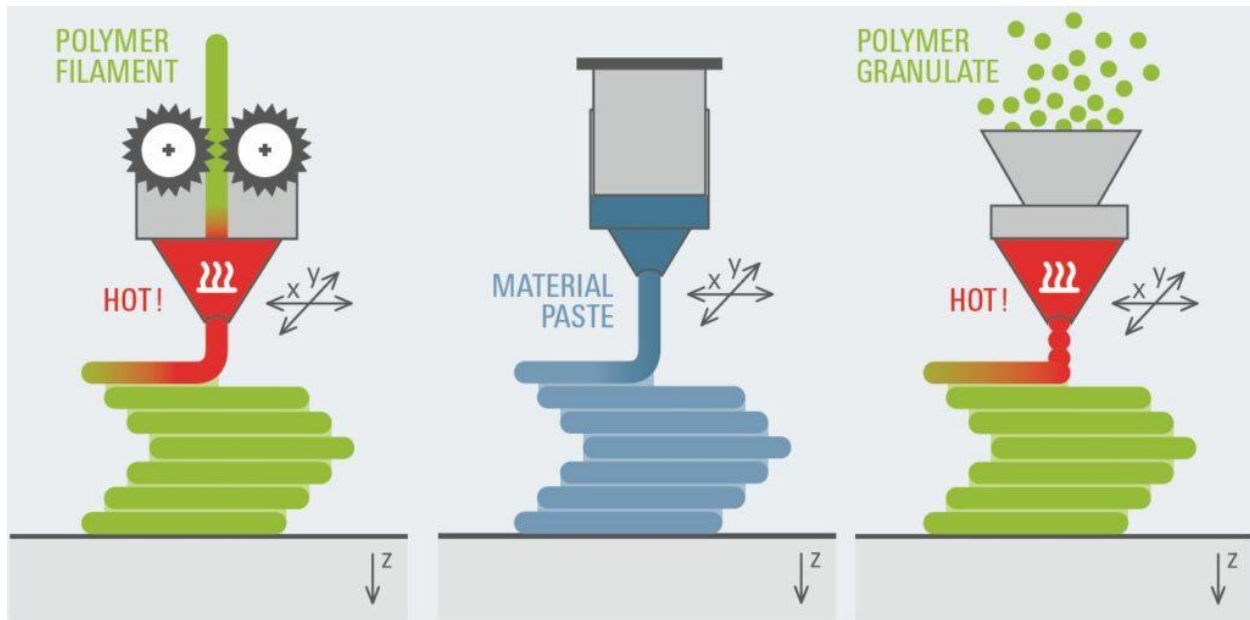
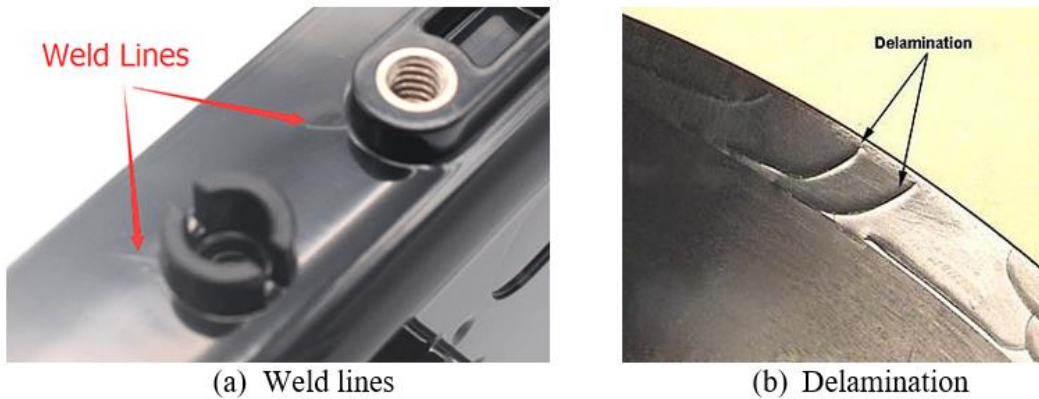


Figure 25: FFF/MEX 3D printing technology [18].

Other forms of additive manufacturing such powder bed fusion (PBF), binder jetting (BJT), and directed energy deposition (DED) are not explored in this study since they have higher cost and lower feedstock choice flexibility compared with MEX. MEX is capable of processing standard and high-performance materials including PLA, ABS, nylon, and PEEK. Moreover, it can process polymeric filaments reinforced with short and continuous fibers, e.g., carbon and glass. When producing complex geometrics, the support material deposition is designed by software (and then implemented in the print) to hold overhangs present during printing. The presence and need for support material add to the amount of material waste to produce a part.

To further discuss the efficacy of the different manufacturing methods, this study also describes some of the major defects involved in each method. Some of the common injection molding defects include flow lines, sink marks, weld lines, burn marks, discolouration, delamination, flashes, and short shots. They have their corresponding effect on the structure, cause, and method of troubleshooting. The most detrimental defects during injection molding process includes weld lines and delamination (see Figure 26). Weld lines are characterized as localized streaks of converged molten material on the surface of the part and occur due to weak material bonding [19]. Delamination, a phenomenon whereby the thin surface layers separate, is a relatively consequential defect that ultimately reduces the strength of the molded component. It is caused by using incompatible polymers, using excessive amounts of release agents, and/or having excessive moisture during molding [19]. Despite having consequential effects, these defects may be easily prevented using proper manufacturing and material storage techniques. Compression molding shares a lot of the same types of defects since it also involves fitting material within a mold; nevertheless, compounds undergoing compression molding are more susceptible to warping due

to uneven distribution of temperatures during compression and curing [12]. In addition, small distortions or breaks are outcomes of molding overly complex geometries via compression.



*Figure 26: Occurrences of (a) weld lines, and (b) delamination [16].*

Additive manufacturing, on the other hand, brings about many distinct issues in manufacturing when compared to compression and injection molding. Since the process involves fabrication in an upwards direction, one major defect whilst printing may void the entire part. Print quality is a large determinant of successfully printed parts since they may alter their performance. Some typical symptoms of poor 3D printing include scars, warps, gaps, layer shifts, and layer separation [20]. Though there are many forms of defects, layer separation and gaps between infill and outline are defects that strongly decrease the overall strength of a part (see Figure 27).

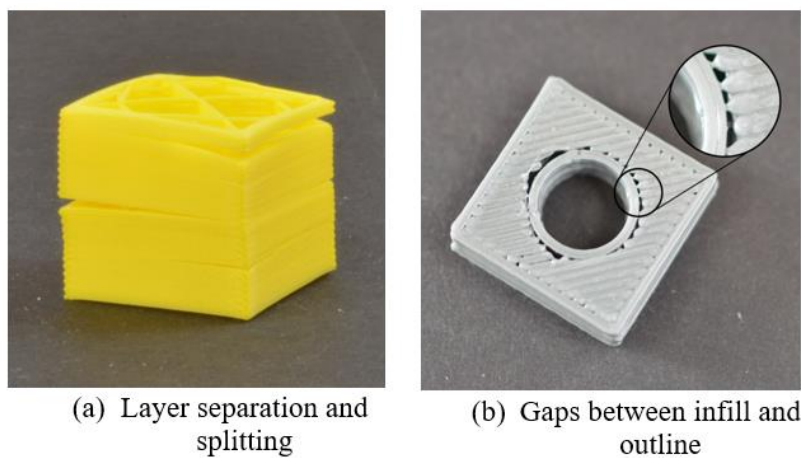


*Figure 27: Occurrences of defects in 3D printed parts: (a) layer separation and splitting; and (b) gaps between infill and outline [20].*

Typically, these issues are resolved by making sure that the temperatures and extrusion rates are selected to suit the type of material used. Layer separation and splitting are the results of large

layer heights. Gaps between infill and outline are the results of too low of an “outline overlap” value or too high of a printing speed [20]. Many parameters must be adjusted to cater to each print. This is an indication of the complex issue of finding the optimal settings for 3D printing specific materials and specific shapes. One of the greatest concerns for all applications where MEX/FFF is used is the adhesion between layers of filament as they are stacked in the +z direction. The interface between printed filament strings as they are laid over one another creates lines of potential failure in the form of layer separation.

The defects that were mentioned are important considerations when exploring the feasibility of the different manufacturing methods since they determine the reliability of each method. After exploring the three principal manufacturing methods selected as candidates for the design of a drone body, it was possible to form a comparison between them. Table 4 demonstrates the advantages and disadvantages of using each type of manufacturing method for drone frame manufacturing [15, 16, 21].

*Table 6: Advantages, disadvantages, and suitable materials of various manufacturing methods*

<b>Manufacturing Method</b>	<b>Advantages</b>	<b>Disadvantages</b>	<b>Suitable Materials</b>
<b>Compression Molding</b>	<ul style="list-style-type: none"> <li>• Ease of maintaining mold tooling</li> <li>• Low initial tooling costs and investment</li> <li>• Enables efficient colour changeovers</li> <li>• Preserves mechanical and chemical properties of materials</li> <li>• Ensures better visual appearance by avoiding gate vestige</li> </ul>	<ul style="list-style-type: none"> <li>• Slightly less consistent than injection molding</li> <li>• Not well suited for complex parts or large production runs</li> <li>• Products may show odd parting lines</li> <li>• Secondary machining may be required</li> <li>• Reduced molding depth</li> </ul>	<ul style="list-style-type: none"> <li>• Diallyl phthalate (DAP)</li> <li>• Thermoset polyester</li> <li>• Epoxy</li> <li>• Sheet molding compound (SMC)</li> <li>• Vinyl ester</li> <li>• Phenolics</li> <li>• Silicone</li> </ul>
<b>Injection Molding</b>	<ul style="list-style-type: none"> <li>• Efficient production of uniform components</li> </ul>	<ul style="list-style-type: none"> <li>• High tooling cost</li> <li>• Only cost-efficient when</li> </ul>	<ul style="list-style-type: none"> <li>• Polyethylene</li> <li>• Polystyrene</li> <li>• Nylon</li> </ul>

	<ul style="list-style-type: none"> <li>• Allows molding of secondary features</li> <li>• High degree of versatility and customization</li> <li>• Low production costs</li> <li>• Rigid and durable final products</li> <li>• Able to produce parts of high complexity</li> <li>• Tolerates a wide range of materials</li> </ul>	producing large numbers of products	<ul style="list-style-type: none"> <li>• Polypropylene</li> <li>• Acrylonitrile butadiene styrene (ABS)</li> <li>• Polycarbonate</li> </ul>
<b>Additive Manufacturing</b>	<ul style="list-style-type: none"> <li>• Much of the supply chain's intermediate steps are removed</li> <li>• Set-up costs are greatly decreased</li> <li>• Ability to create objects with functionally-graded materials</li> <li>• Ability to create complex geometries</li> <li>• Ability to create small lot sizes</li> <li>• Allows for different material properties at different locations</li> </ul>	<ul style="list-style-type: none"> <li>• Expensive machinery</li> <li>• Impractical for manufacturing large lot sizes due to time constraints</li> <li>• Requires extensive post-processing to clean and smooth out the object</li> <li>• May create a large quantity of waste material depending on the complexity of structure</li> <li>• Hard to compute the structural properties of geometry due to</li> </ul>	<ul style="list-style-type: none"> <li>• PLA</li> <li>• ABS</li> <li>• PETG</li> <li>• PVA</li> <li>• Nylon</li> <li>• Wood composite</li> <li>• HIPS</li> <li>• Metal composite</li> <li>• Resins</li> </ul>

---

complexities in  
internal structure  
and a large  
number of  
possible defects

---

Table 5 summarizes the criteria used for determining the most suitable manufacturing method for different applications:

*Table 7: Ranking criteria used for manufacturing method selection.*

<b>Criteria</b>	<b>Description</b>	<b>Weight (%)</b>
<b>Ability to Produce Complex Parts</b>	The ability to produce complex parts describes the manufacturing method's ability to reliably create parts with many indentations and small details. Complexity is also used to describe the presence of internal geometries. A higher ability to produce complex parts is desired.	13.48
<b>Ease of Usage</b>	Ease of usage describes the user-friendliness of the machines used in each manufacturing technique as well as all third-party software knowledge required to use the technique. This also ties in with the manufacturability of a part since some machinery may not require much user input. Easier usage is desired.	6.18
<b>Cost Effectiveness</b>	Cost-effectiveness refers to the cost of producing the parts as well as the costs associated with production. This may include the cost of the machines, operating the machines, and the production of machine parts needed to produce the outcome. Higher cost-effectiveness is desired.	7.30
<b>Reliability</b>	Reliability is defined as the ability to perform as expected and yield expected results with as minimal defects as possible. Reliability is tied in with the method's ability to retain material properties. Reliability also encapsulates the ability of the method to produce as many parts as possible before repair, maintenance, or replacement. Higher reliability is desired.	14.04
<b>Ability to Produce Prototypes</b>	The ability to produce prototypes describes the feasibility to produce prototypes. Questions of how fast, effectively, and reliably a preliminary part may be produced are explored by this criterion. A higher ability to produce prototypes is desired.	6.74
<b>Ability to Mass Produce</b>	The ability to mass produce refers to the method's feasibility to produce several repeated products. The consistency, as well as	7.30

	the speed by which the products are produced, are discussed by this criterion. A higher ability to mass produce is desired.	
<b>Need for Post-processing</b>	The need for post-processing describes the amount of work required after using the manufacturing method to complete the product. If a manufacturing method can return a finished product without the need for post-processing, then additional costs and time are reduced; in addition, this means there is less possibility of error in processing since most issues would be centered around the method. A lower need for post-processing is desired.	8.99
<b>Ability to Retain Material Properties</b>	The ability to retain material properties is strongly correlated with the reliability of the manufacturing method. Since different materials are more or less suited for different methods, a material chosen for specific properties should exhibit those properties in a product after production. A higher ability to retain material properties is desired.	12.92
<b>Waste Material Production</b>	Waste material production refers to the undesired outcome (waste) material that the method produces; this ensures that less funding and time is spent on recycling and disposal initiatives. This criterion also ensures the products and production processes are eco-friendly. Lower waste material production is desired.	9.55
<b>Ability to Use Engineering Materials</b>	The ability to use engineering materials describes the manufacturing method's capacity to produce geometries made of strong, functionally graded materials specifically engineered for given objectives. A higher ability to use engineering materials is desired.	13.48

The numerical weight assigned to each was assigned according to what was believed to hold the greatest accreditations for flight readiness according to the method described in [9]. Reliability of the manufacturing method, for example, was given the greatest priority.

The manufacturing method was selected based on the criteria and weightings described in Table 7. Figure 28 demonstrates the rankings of each body type according to Table 7 and calculations presented in Table 24 in Appendix A:

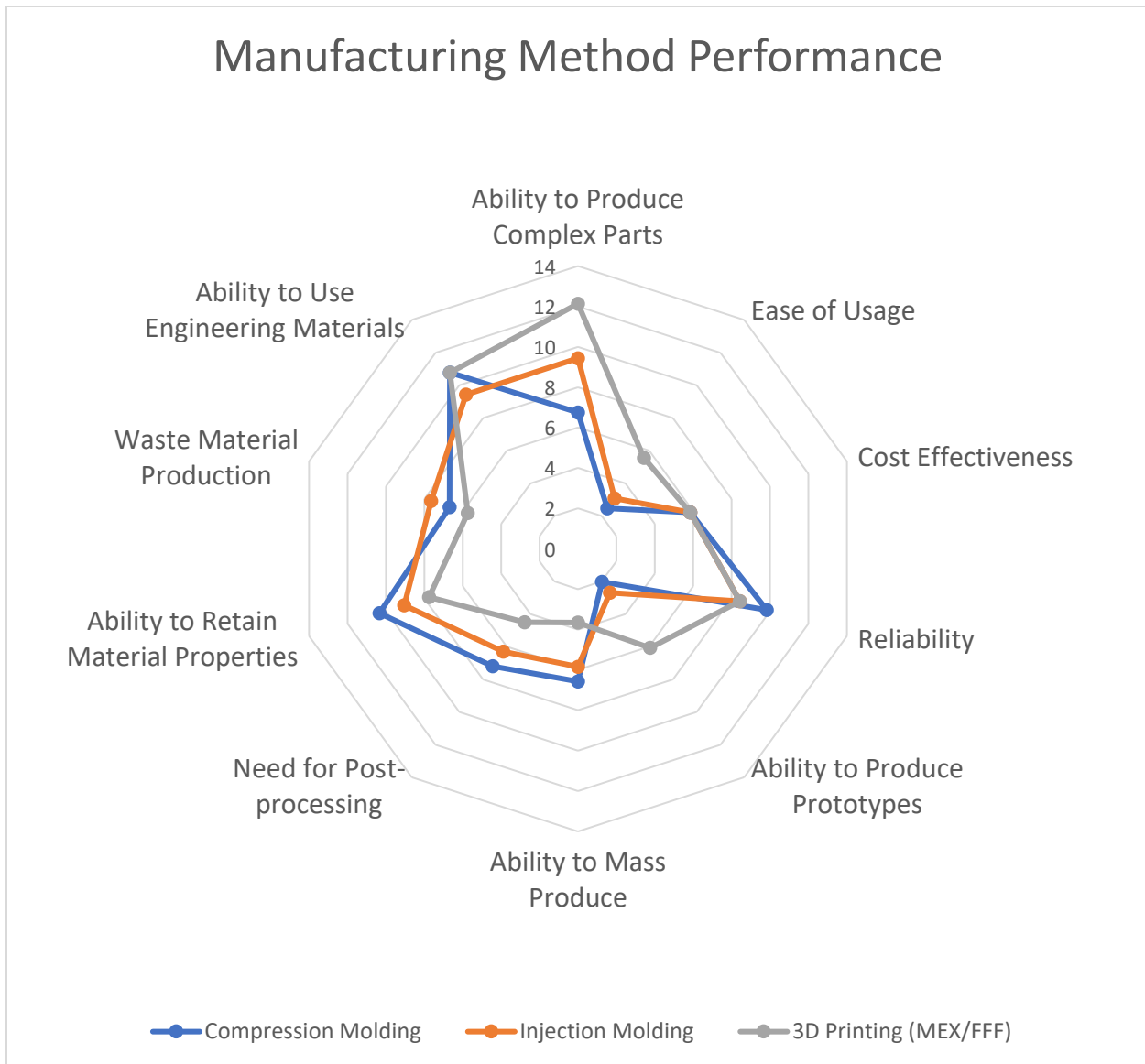


*Figure 28: Attribute ranking for manufacturing methods.*

The method of manufacturing demonstrating the highest results according to the criteria described in Table 7 was found to be 3D printing (MEX/FFF). It scored 70.4% in its applicability to the study.

### 4.3 Material

The material selected for exploration has a vital operation in the success of a quadcopter drone frame. The materials chosen to comprise the body must be able to sustain the loads applied by the weight and thrust shown in Figure 19. The materials must be carefully selected to cater to the geometry of the frame since localized forces exhibit the greatest points of failure. In addition, the manufacturability of the frame will be impacted because some manufacturing methods are more

suitable for certain materials). Based on the information gathered in Sections 4.1 and 4.2 regarding the drone frames and manufacturing methods, i.e., MEX, the potential candidate materials for study were selected:

- Acrylonitrile butadiene styrene (ABS)
- Polylactic acid (PLA)
- Polycaprolactam (PA) (also known as Nylon 6)
- Polypropylene (PP)
- Polystyrene (PS)
- Polycarbonate (PC)
- Thermoplastic polyurethane (TPU)
- Acrylic Styrene Acrylonitrile (ASA)
- Polyethylene terephthalate glycol (PETG)
- Polyetheretherketone (PEEK)
- Polyetherketoneketone (PEKK)
- Polyetherimide (PEI)

To explore any characteristic patterns in material properties, the materials that were selected may be separated and classified. In the following material categorizing chart, “TP” denotes thermoplastic, “TS” denotes thermoset, “A” denotes amorphous, and “SC” denotes semi-crystalline.

*Table 8: Material classification; adapted from [22].*

<b>Material</b>	<b>Type of Plastic</b>	<b>Crystallinity</b>	<b>Availability</b>	<b>Grade</b>
<b>ABS</b>	TP	A	Commercial	Commodity
<b>PLA</b>	TP	SC	Commercial	Engineering
<b>PA</b>	TP	SC	Commercial	Engineering
<b>PP</b>	TP	SC	Commercial/Scientific	Commodity
<b>PS</b>	TP	A	Scientific	Commodity
<b>PC</b>	TP	A	Commercial	Engineering
<b>TPU</b>	TP	SC	Commercial	Engineering
<b>ASA</b>	TP	A	Commercial	Engineering
<b>PETG</b>	TP	A	Commercial	Engineering
<b>PEEK</b>	TP	SC	Commercial	High Performance
<b>PEKK</b>	TP	SC	Not Available	High Performance
<b>PEI</b>	TP	A	Commercial	High Performance

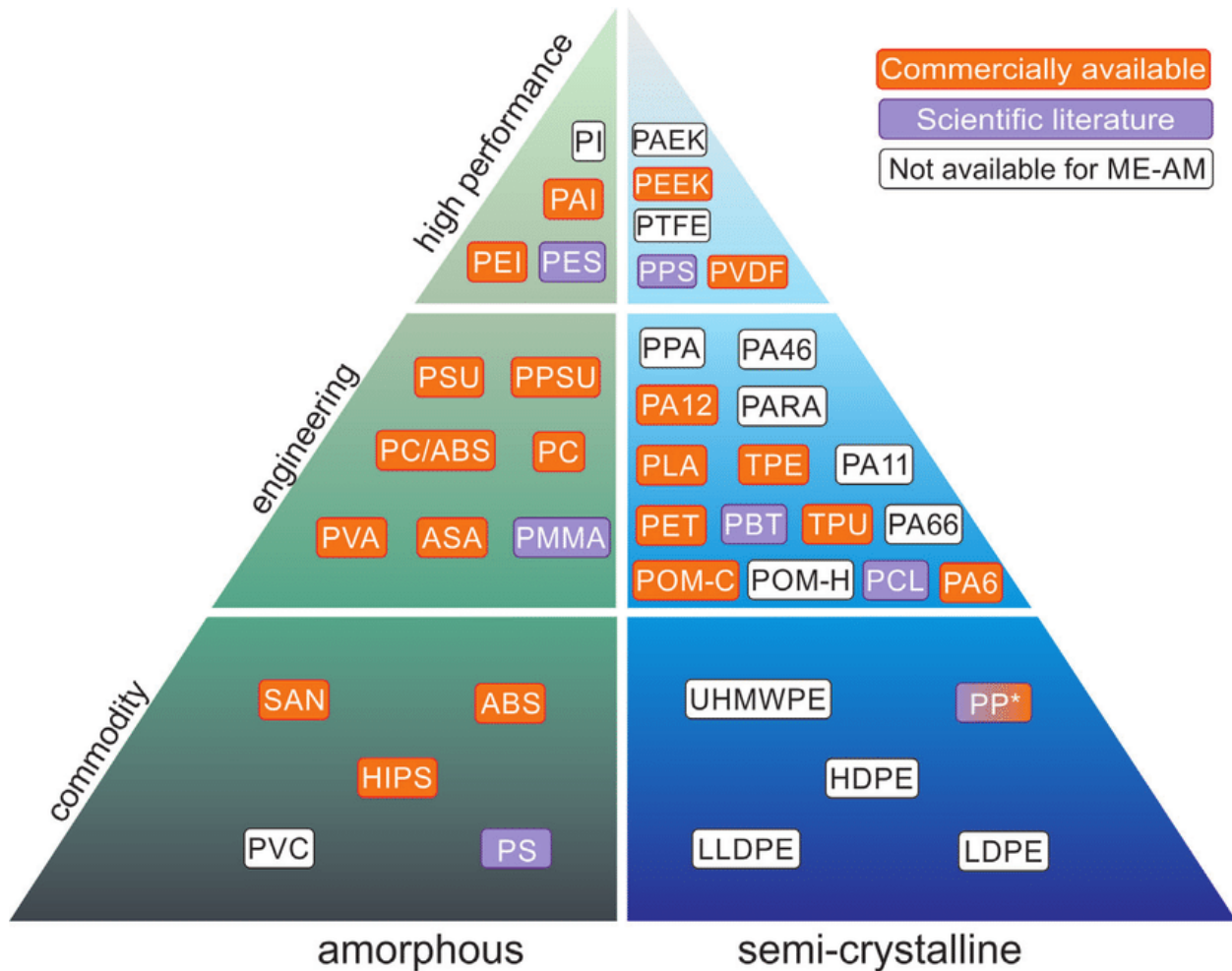
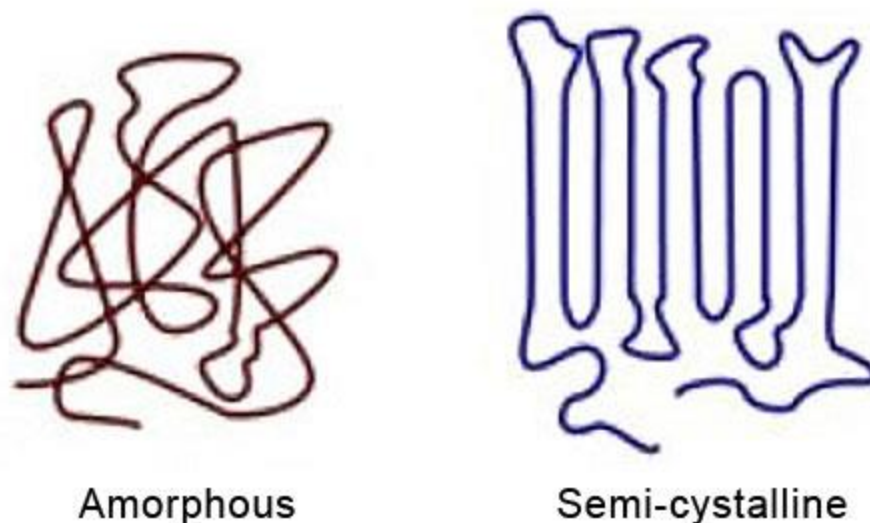


Figure 29: Pyramid of polymeric materials in terms of availability, amorphous/semi-crystalline, and performance [22].

Amorphous materials are those which do not exhibit an organized molecular structure; the random molecular structure lacks a sharp melting point [23]. The lack of ordered structure allows gradual softening with increasing temperatures. In addition, amorphous materials demonstrate lower mechanical strength and stiffness, yet greater flexibility and lower brittleness compared to crystalline polymers [23]. Crystalline and semi-crystalline polymers exhibit characteristics expected from ordered molecular structures. For semi-crystalline materials, a low-viscosity liquid is achieved at temperatures generally higher than the upper range of amorphous thermoplastic. A representation of the alignment of molecules in both types of plastics is shown in Figure 30.



*Figure 30: Amorphous versus semi-crystalline material molecular chain structure [24].*

Their respective molecular patterns highly dictate the performance of each type of polymer. Amorphous polymers show high attraction between polymer chains, are generally high in density, have low chemical resistance, and are transparent [23]. Semi-crystalline polymers show weak attraction between polymer chains, are generally low in density, have high chemical resistance, and are translucent. Both types of plastics have different suitable applications. Table 9 demonstrates the major advantages and disadvantages of amorphous versus semi-crystalline plastics.

*Table 9: Advantages and disadvantages of amorphous and semi-crystalline polymers [23].*

Crystallinity	Advantages	Disadvantages
<b>Amorphous</b>	<ul style="list-style-type: none"> <li>• Easy to thermoform</li> <li>• Better dimensional stability than semi-crystalline plastics (less likely to warp) due to isentropic flow nature</li> <li>• Superior impact strength which makes them suitable for structural applications</li> <li>• Bond well using adhesives</li> <li>• Resistant to heat, moisture, chemicals</li> <li>• Generally high in stiffness and strength</li> </ul>	<ul style="list-style-type: none"> <li>• More prone to stress cracking due to their hydrocarbon make-up</li> <li>• Do not perform well in applications of wear</li> <li>• Poor fatigue resistance</li> <li>• Lower chemical resistance than semi-crystalline materials</li> <li>• Higher friction (surface roughness) than semi-crystalline materials</li> </ul>

<b>Semi-Crystalline</b>	<ul style="list-style-type: none"> <li>• Tough due to their strong intermolecular forces</li> <li>• Perform well in applications of wear such as in bearings and structural loads</li> <li>• Better resistance to chemicals compared to amorphous materials</li> <li>• Generally higher stiffness, strength, and toughness than amorphous materials</li> <li>• Very low coefficient of friction</li> </ul>	<ul style="list-style-type: none"> <li>• Sharp melting points make them difficult to thermoform</li> <li>• Due to its anisotropic flow nature, the material warps by shrinking in the direction transverse to flow more than the direction of flow</li> <li>• Dimensional instability compared to amorphous polymers</li> <li>• Lower impact resistance than amorphous materials</li> <li>• Hydrophobic</li> </ul>
-------------------------	--	--

Based on the information obtained in exploring the different materials from both theoretical knowledge and literature review, it was possible to generate a list of criteria by which the chosen materials may be ranked. For the sake of this study, the following list of mechanical properties (which form the criteria) was used to judge each candidate material:

*Table 10: Ranking criteria used for material selection.*

<b>Criteria</b>	<b>Associated Test/Property</b>	<b>Unit</b>	<b>Description</b>	<b>Weight (%)</b>
<b>Impact Resistance</b>	Charpy Impact (Unnotched)	J/cm <sup>2</sup>	The Charpy impact test is a standardized means of characterizing a material by its ability to absorb high strain rate impact energy. Impact resistance is the ability of a material to absorb impact energy. A higher degree of impact resistance is desired.	17.86
	Density	g/cm <sup>3</sup>	The mass of the material has a strong implication on the drone's success in flight. Lower-density materials have less weight for the same amount of volume, which ultimately results in a less heavy structure. Lower-density materials are desired.	16.97
<b>Mass</b>	Modulus of Elasticity	GPa	Stiffness describes a material's ability to resist deformation in response to an applied force. Stiffness must be controlled in the case of drone design since high stiffness incites brittleness and low stiffness incites	11.61
<b>Stiffness</b>				

			instability. In this study, higher modulus of elasticity values are desired.	
<b>Heat Resistance</b>	Deflection Temperature at 0.46 MPa, Maximum Service Temperature (Air)	°C	Heat resistance describes a material's ability to survive high-heat environments for long exposures. Two characteristics of heat resistance include deflection temperature and maximum service temperature. Higher heat resistance is desired by demonstrating lower deflection temperature and higher service temperature.	13.39, 11.61
<b>Strength</b>	Ultimate Tensile Strength (UTS), Yield Tensile Strength (YTS)	MPa	Strength describes the ability of a material to resist failure by fracture or yield in the presence of an applied quasistatic stress. Two characteristics, UTS and YTS, were used to determine strength. Higher strength values are desired.	8.04, 7.14
<b>Water Resistance</b>	Water Absorption	%	Water resistance refers to the material's ability to survive long exposures to water. In the case of this study, lower water absorption as a percentage of the total mass is desired.	13.39

Unlike frame-type and manufacturing-method selections, the selection for the material was based on numerical test values documented in literature. Therefore, an indexing method of assigning normalized rankings to each material property (for each material) was required. Fayazbakhsh et al. [9] describes a method of selecting materials that satisfies the current study application. Utilizing the Z-transformation normalization process described in [9], Figure 31 was generated to describe the performance of each material:

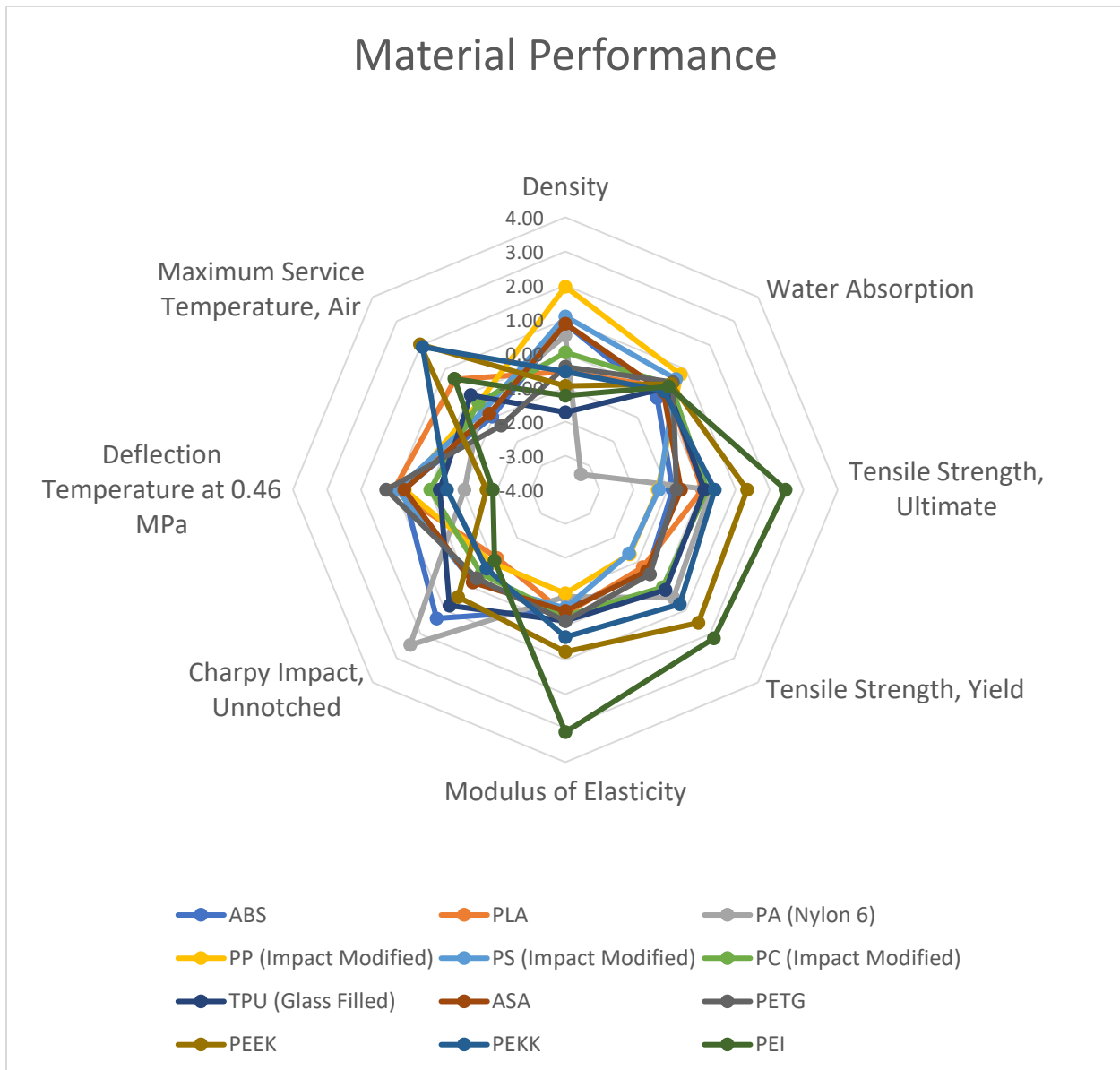


Figure 31: Attribute ranking for materials.

The numerical weight assigned to each was assigned according to what was believed to hold the greatest accreditations for flight readiness according to the method described in [9]. Impact resistance via the Charpy impact test (unnotched), for example, was given precedence. Results from the study for material selection were as follows: PEEK was found to have the greatest score mainly due to its high thermal resistance (specifically maximum service temperature). ABS held the second spot due to its high impact resistance. PEI held the third position due to its high modulus of elasticity and strength. Table 27 in Appendix A

All selection processes involved using the decision matrix displayed in Table 21, Table 23, and Table 25 for geometry, manufacturing method, and material respectively. In these tables, the goals

are compared one-to-one; if it is believed that one goal holds more value than its competitor, then the more valuable goal is assigned a value of 3 whereas the less valuable goal is assigned a value of 1. If both goals are of the same value, both are assigned a value of 2. Adding all of the positive decisions of one attribute and dividing the sum by the total number of positive decisions yields the weighting factor. In the geometry and manufacturability rankings, the weighting factor is multiplied to a score out of 1. The score was given using best judgement based on knowledge. In the material ranking, normalization was done by applying Z-transformation. The sum of normalized properties multiplied by respective weightings presented the performance index. A details the Z-transformation indexing process.

## 5.0 Design Process

After exploring literature as well as reviewing theoretical knowledge on all three aspects of successful drone design (geometry, manufacturability, and material), a preliminary conceptual design was generated. The conceptual design attempted to consider the trade-offs associated with the interdependencies between geometry choice, manufacturing method choice, and material choice. From Sections 4.1, 4.2, and 4.3 the following combination was chosen for study: A generatively designed square-framed drone made of PEEK and manufactured via MEX/FFF 3D printing.

### 5.1 General Design Considerations

This section explores the possible designs for the drone frame considering the information learned from previous sections. More specifically, this section discusses a potential plan for designing, computing, and realizing a physical prototype of a quadcopter. It should be noted that due to limited resources, the combination of ideal geometry, manufacturing method, and the material was not possible. The specific issue was that PEEK was not readily available to be 3D printed at FRAMES since (1) PEEK was not ordered, and (2) 3D printer set-up was not done. The following table lists the decisions made for the potential drone design:

*Table 11: Decisions made for the conceptual design and reasonings for each decision.*

#	Decision	Reasoning
1	The drone frame shall be dictated by a “square” and/or “true-X” geometry.	Square and True-X frames are symmetrical about four planes which makes them simple and easy to manufacture. In addition, they provide stability in flight and ensure even distribution of force load across each propulsion system and weight of components.
2	“Beam” connections shall be made between each arm and the centre body of the drone.	Multiple beams forming arms allow for even distribution of force along the frame of the drone. The beams shall

		also connect each tip of the arm to increase the distribution of load.
<b>3</b>	“Beam” cross-sections shall not be limited by design to only have one geometry.	The number of fracture points along each arm shall be reduced by implementing variable geometry along each “beam” forming the arms.
<b>4</b>	Fillets shall be present wherever conjoining between different regions of the drone are seen.	Fillets between arm and propulsion system supports as well as between arm and centre body allow for less localized forces in weak areas.
<b>5</b>	The drone shall be unibody.	Designing a unibody drone not only simplifies the manufacturing process (since no screws, bolts, nuts, adhesives, and locking mechanisms would be required), but also reduces the likelihood of failure in what would be the interconnection points.
<b>6</b>	The drone frame shall consider spacing, and geometries, required for mounting equipment.	By considering the spacing required for multiple equipment, problems associated with limited spacing and improper fittings can be reduced.
<b>7</b>	The drone frame shall consider holes and chamfers meant to facilitate the connection of standard-type bolts and nuts where applicable.	Using standard nuts and bolts, the design of the drone may ensure that proper installation and assembly is possible without additional complications and needs for post-processing.
<b>8</b>	The drone shall be designed using Fusion 360’s generative design capability.	Generative design shall be used since it is the purpose of study. Generative design should, in theory, confirm all of the predictions made throughout literature and theory review.
<b>9</b>	The drone shall be manufactured using a FFF 3D printer.	This method of manufacturing was the most readily available and simple. In addition, it was chosen as the most suitable manufacturing method according to the believed standard for flight readiness.
<b>10</b>	The drone shall be made of PLA plastic.	Despite concluding that PEEK is the most suitable candidate material, due to the unavailability of PEEK at this stage, PLA was chosen to be the prototype material.
<b>11</b>	The drone sizing shall be similar to those of hobbyist racing drones. The drone sizing shall be no larger than 200mm by 200mm by 100mm	The preliminary sizing was chosen to be relatively small due to greater ease in manufacturing and time saved. The 3D printer chosen for printing did not have a large enough bed for printing the full-scale drone.

in length, width, and weight respectively.

## 5.2 Preliminary Load Calculations

In order to establish an accurate rendition using generative design, it was necessary to establish an appropriate estimate for the loads the drone would experience in flight. To begin estimating, it was necessary to formulate an approximate sizing for the drone. In this study, hobbyist drone sizing was chosen to dictate the general sizing and weight of the prototype due to its relatively small size and feasibility to be manufactured additively (3D printed). The loads applied to the generatively designed case were chosen in conjunction to the load discussion in Section 4.1.

The predominant load case for exploration was that which satisfied a “pull-up” maneuver in which the drone would have to recover from free-fall before hitting the ground.

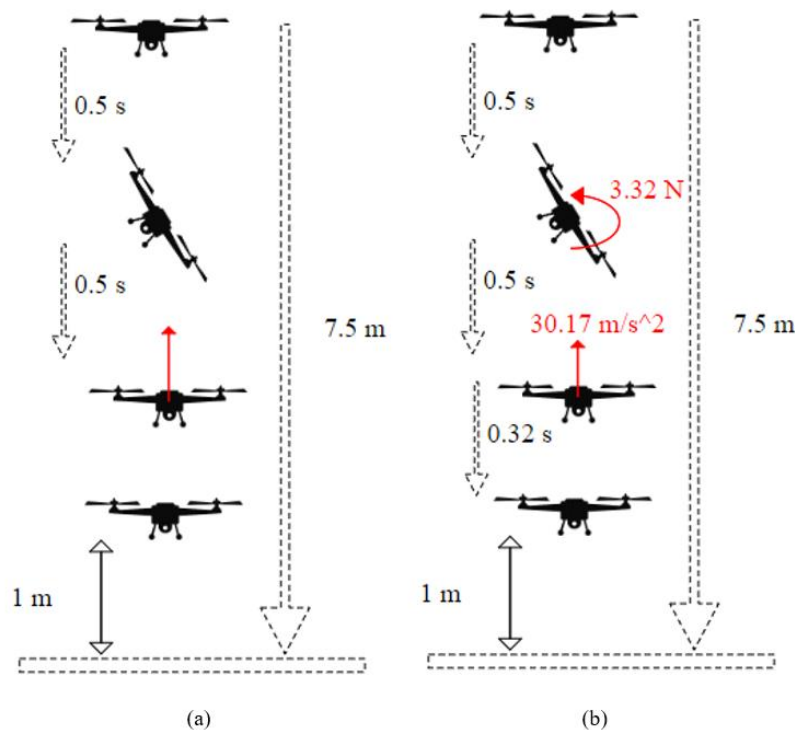


Figure 32: Pull-up maneuver (a) process, and (b) process with calculated loads.

The pull-up maneuver used in estimating the applicable loads for later input to generative design consists of four phases. Phase, phase description, and assumptions made are described in the following table:

Table 12: Pull-out maneuver phases, descriptions of phases, and assumptions made.

Phase Number	Phase	Description	Assumptions
1	<b>Initial Drop</b>	The initial drop information describes the start time and height from which the drone is dropped. A specific height is specified.	The drone begins descension at $t = 0s$ , $v_i = 0m/s$ , and $h_i = 7.5m$ . The mass of the drone was taken to be $m = 1kg$ . The drone was assumed to have four arms each with a length of $l = 0.084m$ .
1-2	<b>Reaction</b>	Time is allocated to consider latency due to reaction time by either user or program controlling the drone.	The drone undergoes free fall without external forces for $t_r = 0.5s$ .
2-3	<b>Moment</b>	Time is allocated to consider any re-orientation maneuvers that must occur before the drone can generate thrust directly opposite to its direction of travel.	The drone is oriented such that it cannot provide direct upwards thrust meaning that a moment must be created by activating one or more turbines. The propellers can only generate thrust in one direction. No upwards thrust contributes the deceleration of the drone in the reorientation process. The drone undergoes free fall without external forces for $t_m = 0.5s$ . It is assumed that the reorientation occurs constantly through the time.
3-4	<b>Landing</b>	The drone begins a thrust maneuver to generate enough upwards thrust to cease it from falling some offset distance away from the ground.	A set amount of space from the ground is parameterized in order to find the force necessary to decelerate the drone to $v_f = 0m/s$ at a distance from the ground of $h_l = 1m$ .

The scenario described above was used in order to apply realistic loads to the drone which is to be generatively designed. The results from applying the assumptions stated in Table 12 to the scenario in Figure 32 may be seen below:

Table 13: Pull-out maneuver phase and result per phase.

Phase Number	Phase	Results	Reference Equation
1	Initial Drop	The initial conditions show that the time and distance remaining are: $t_{r,i} = 1.2365s$ $h_{r,i} = 7.5m$	8
1-2	Reaction	After finishing the reaction portion of the drop, the time and distance remaining is: $t_{r,1} = 0.7365s$ $h_{r,1} = 6.2737m$	8
2-3	Moment	After applying a moment for the specified time to re-orient the drone, the time and distance remaining is: $t_{r,2} = 0.2365s$ $h_{r,2} = 2.5950m$ The force experienced at the end of each arm due to centrifugal force is: $F_c = 3.3162N$	8, 9
3-4	Landing	Given the calculated conditions after the drone has re-oriented, the acceleration required to stop the drone the set distance away from the ground is: $a = 30.1681m/s^2$ Which corresponds to a load-per-arm of: $F_p = 7.5420N$ In the case where one rotor is inoperable, each arm must produce: $F_{p,3rotors} = 10.0560N$ Therefore: $v_f = 0m/s$ $t_f = t_{r,i} = 1.2365s$ $h_{r,f} = 1m$	8, 9

The equations that were used in finding the various parameters shown in Figure 32 and Table 13 may be seen at the end of this section. The calculative investigation that was conducted by means of exploring the pull-out maneuver demonstrated realistic results when compared to the forces experienced by the theoretical drone referred to in Section 4.1. These loads were calculated only by establishing estimates of possible drone parameters such as sizing and weight. In order to establish the “worst-case-scenario”, and hence considering for a wider range of operability, the

three-rotor-operable case was used in determining forces applied to the drone. In addition, a safety factor of two was set for the generative design load cases which are explored in Table 14.

Though the analysis done only explored one possible load case, there are many other loads cases that must be considered. For example, maximum-thrust lift-off, sharp turns, change of flight direction, and maximum horizontal speed cases may also be explored for loads. Moreover, impact behaviours of various drone frames must also be modelled to establish a proper understanding of the loads that drones experience in flight. For the sake of simplicity, and because it falls outside the scope of this study, these additional load cases were not explored.

The solution to the scenario was established using the MATLAB software; the code written for the solution may be seen in Appendix C. The equations that were used to calculate the various parameters shown in Table 13 (and which were implemented to the MATLAB code) fall under the classical mechanical subfield of kinematics as well as Newton's second law of motion:

$$\overrightarrow{\Delta d} = \overrightarrow{v}_i t + \frac{1}{2} \overrightarrow{a} t^2 \quad (8)$$

$$F = ma \quad (9)$$

Using the forces obtained in this section, a generatively designed solution was established; one of the requirements for generative design is to provide the AI with load cases by which it may generate results of potential structures.

### 5.3 Generative Design Outcomes

Generative designing uses artificial intelligence algorithms to compute numerous design solutions for given constraints, loads, preserve geometries, obstacle geometries, and starting shapes. In addition, Fusion 360's generative design capabilities require that goals be set; as such, the AI may attempt to satisfy the goals. In this study, various iterations for loads, constraints, preserve geometries, obstacle geometries, and starting shapes were created. Using the decisions described in Table 11, as well as the theoretical knowledge obtained through study and review of literature, a finalized generative outcome was made. A render of the final design may be seen in Figure 33.



*Figure 33: Render of generative design outcome 1.*

Section 5.3.1 discusses the manner in which the final solution was generated and the reason for which the generative outcome shown in Figure 33 was chosen to represent the physical outcome of this study.

### 5.3.1 Previous Iterations

Before achieving a final solution, five different types of combinations of preserve, obstacle, and in some cases starting geometries were attempted in the process of learning how to use Fusion 360's generative design capability. Figure 34 demonstrates the geometries for the five design iterations:

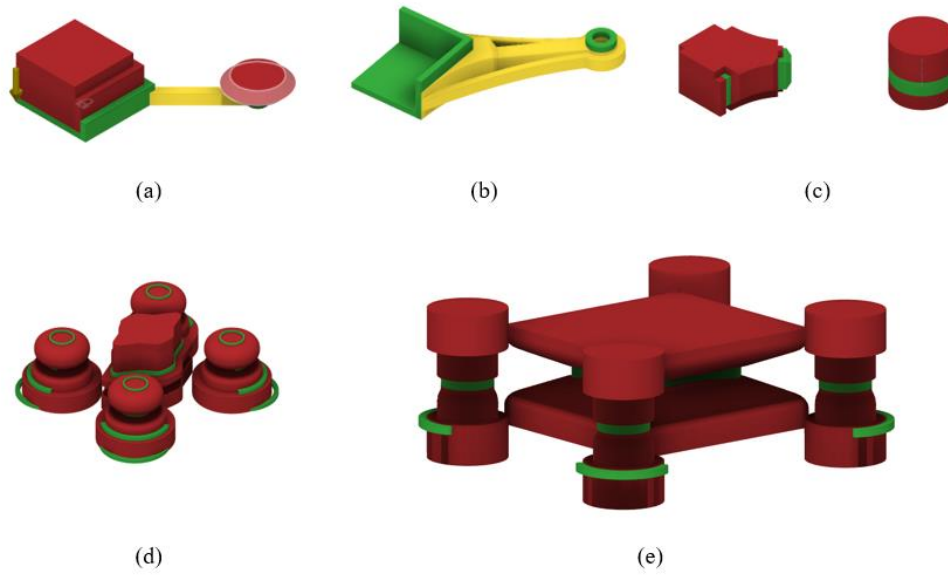


*Figure 34: Generative design iterations showing preserve (green), obstacle (red), and starting (yellow) geometries.*

The first three iterations were only of a singular arm which forms one-fourth of the quadcopter. The other two were attempts at making unibody drones. The last design, Figure 34-(e), yielded the cleanest and simplest results. All other geometry results demonstrated many failed or unsolved iterations. The fifth iteration yielded various possible generative outcomes, each demonstrating various masses, factors of safety, maximum deflection, and Von Mises stresses. Figure 35 shows some examples of converged solutions.

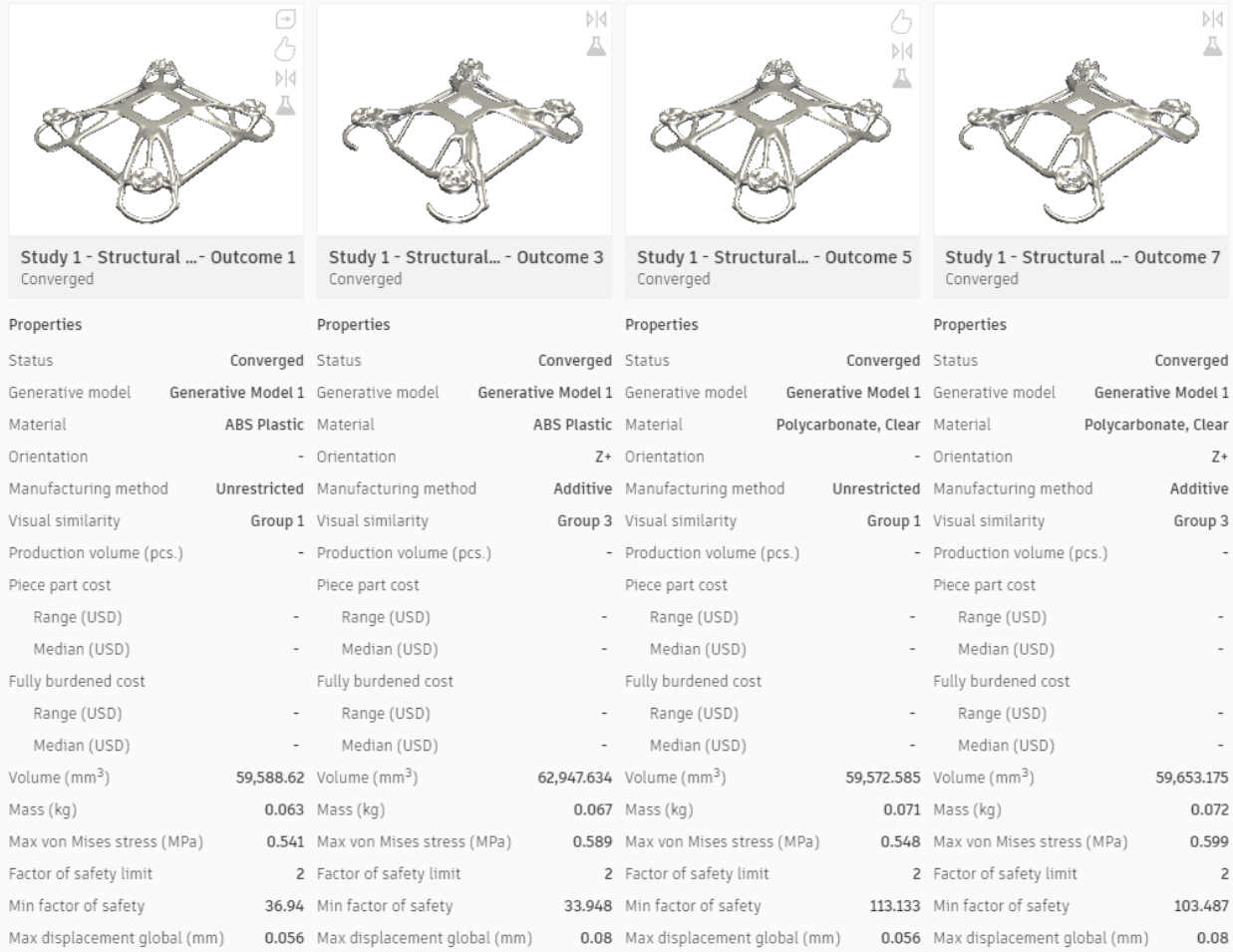


Figure 35: Generative design outcomes 1, 3, 5, and 7 (left to right).

“Outcome 1” is the outcome that was chosen out of the solutions to the fifth iteration shown in Figure 34-(e). Due to the unavailability of PLA as an option, many other types of plastics including ABS, PC, PP, and PC/ABS were used for generative design. The body was set to be unrestricted by any manufacturing method (though additive manufacturing was capable of printing it nonetheless). The volume was found to be 59588.62mm<sup>3</sup>, the factor of safety limit was set to 2, the minimum factor of safety was 37, and the maximum global displacement was found to be 0.056mm. Outcome 1 yielded the most lightweight frame. The settings and parameters (including the loads) that were used for AI computation may be explored in the proceeding section.

### 5.3.2 Settings and Parameters

In this section, the settings and parameters that were applied to the software which allowed for computation are explained in detail. The preserve geometry and obstacle geometry are depicted in Figure 36.

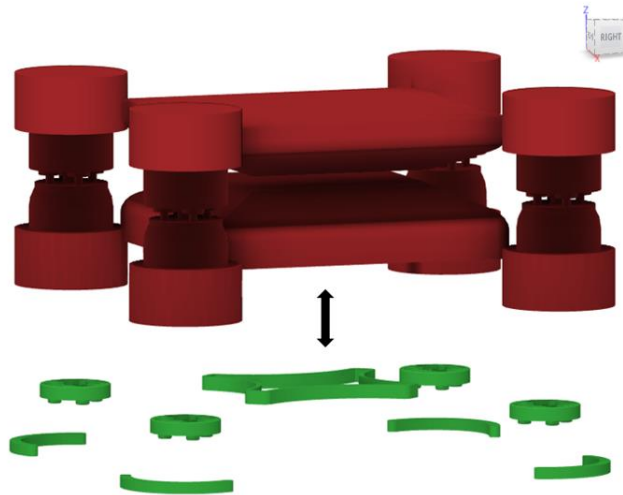
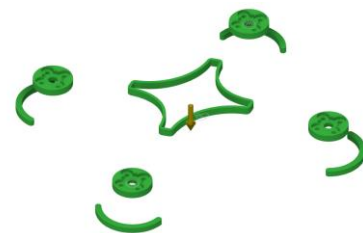


Figure 36: Obstacle and preserve geometries of the fifth iteration.

No starting geometry or obstacle offset geometry was set in computing the generative designs. In addition, two planes of symmetry were imposed on the design—the  $x$ - $z$  plane and the  $y$ - $z$  plane. The objectives that were set were to minimize mass whilst achieving a safety factor limit of 2.00. Two potential manufacturing methods were selected; namely: unrestricted and additive. For both of these manufacturing methods, the materials ABS, PC, PP, and PC/ABS were chosen as the study materials. Four distinct load cases were applied to the preserve geometries; these four load cases are taken as parameters by the AI to generate the most suitable connecting geometries.

Table 14: Load cases applied as settings for generative design computation.

Load Case	Depiction	Constraints	Loads	Applicability in Operation
1		Fixed constraints at the body of each landing gear	20 N downwards load on the top face of the center frame	Heavy mounting equipment applied on top of or below the center frame
2		Fixed constraint at the bottom face of the center frame	5 N upward loads on the top face of each propulsion system interface	Pull-out maneuver where each propulsion system must generate a large amount of almost

				instantaneous thrust
3		Fixed constraint at the bottom face of the center frame	3 N outwards-facing bearing loads within the inner wall of the two opposite corners where the propulsion systems are placed	Centrifugal force applied when the drone must re-orient itself in flight by rotation about the x=y line
4		Fixed constraint at the bottom face of the center frame	3 N outwards-facing bearing loads within the inner wall of the two opposite corners where the propulsion systems are placed	Centrifugal force applied when the drone must re-orient itself in flight by rotation about the x=y line

As may be noted, the preliminary load analysis described by Figure 32 showing the loads experienced by a drone during pull-out were used in the settings for generative design. The sizing parameters chosen for the generative design geometry are shown in the engineering drawing (Figure 37).

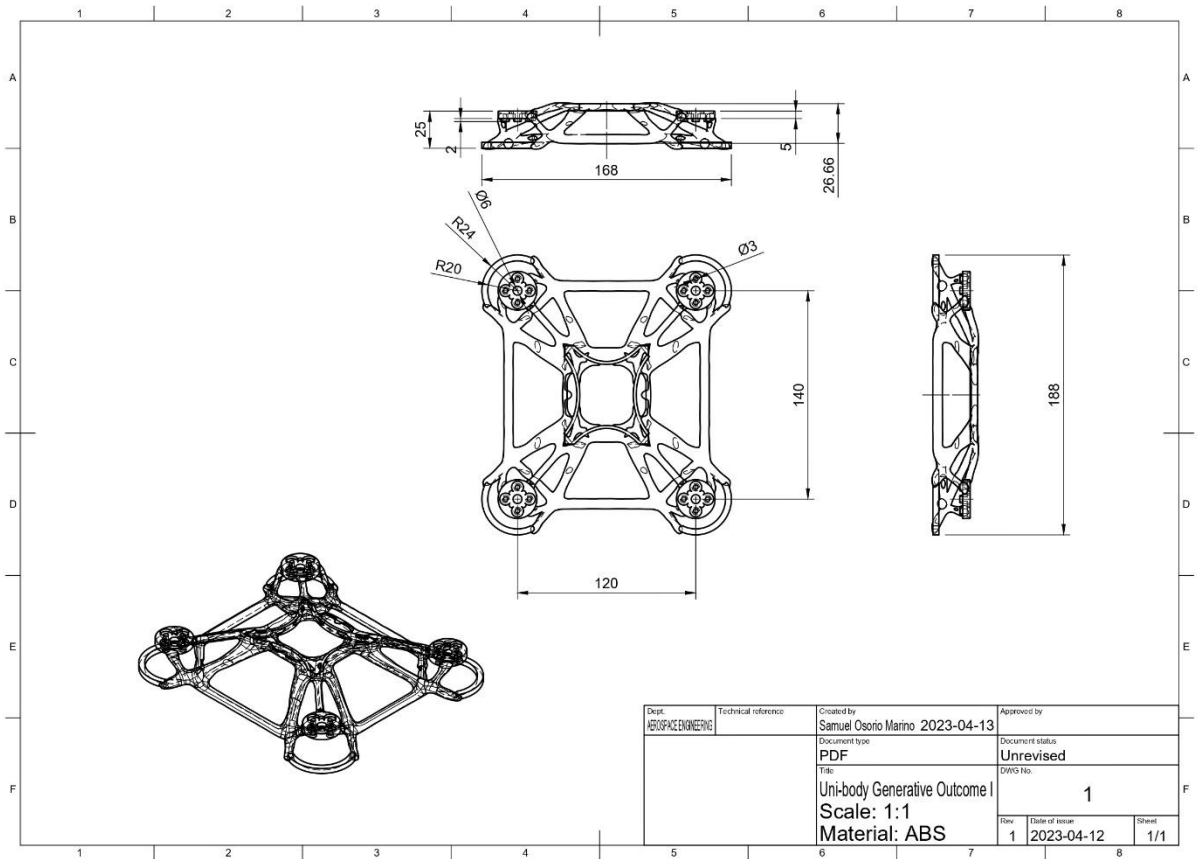


Figure 37: Engineering drawing of outcome 1 showing overall dimensions (mm).

Meshing, which refers to the means by which the geometry is tessellated, dictates the accuracy and precision of FEA analysis. The meshing parameters set for generative design on Fusion 360 are provided in Figure 38.

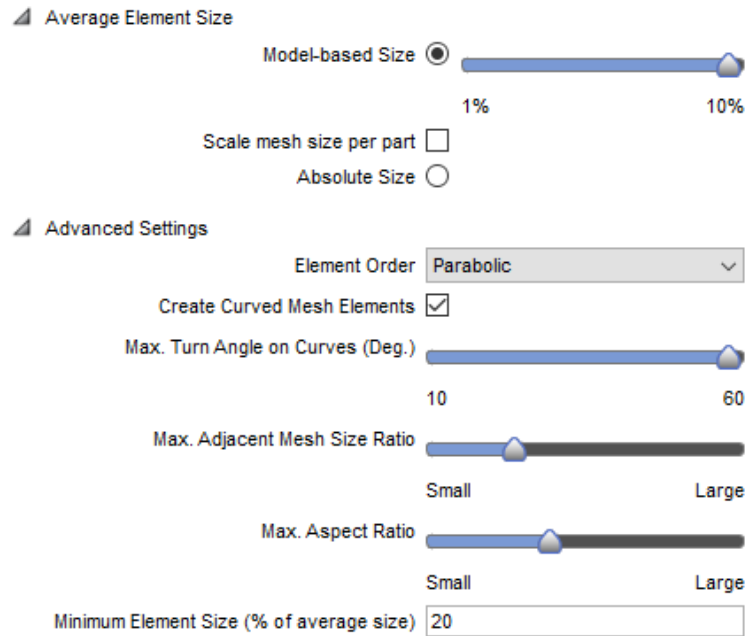


Figure 38: Mesh parameters for generative design outcome 1.

Because the meshing parameters were set for relatively fine tessellation, the results from FEA analysis should accurately represent realistic occurrences to the body of the drone according to the load cases. The results of these loads applied to the geometry may be explored by FEA analysis in Section 5.3.3.

### 5.3.3 Analysis

FEA analysis was done using Fusion 360's FEA capabilities. The loads applied on the first outcome of generative design demonstrated the following distribution of safety factor, Von Mises stress, and displacement:

Table 15: Results from FEA analysis.

Load Case	Minimum Safety Factor	Maximum Von Mises Stress (MPa)	Total Displacement (mm)
1	6.7	2.992	0.0495
2	0.050	401.9	0.517
3	15	0.6581	0.0186
4	15	0.7066	0.0186

The second load case, which is mean to be representative of the upwards force experience during pull-out, demonstrated very unpreferred results. The contour maps generated for factor of safety,

Von Mises stress, and total displacement may be seen in Table 16, Table 17, and Table 18 respectively.

Table 16: Factor of safety contour maps for the four load cases.

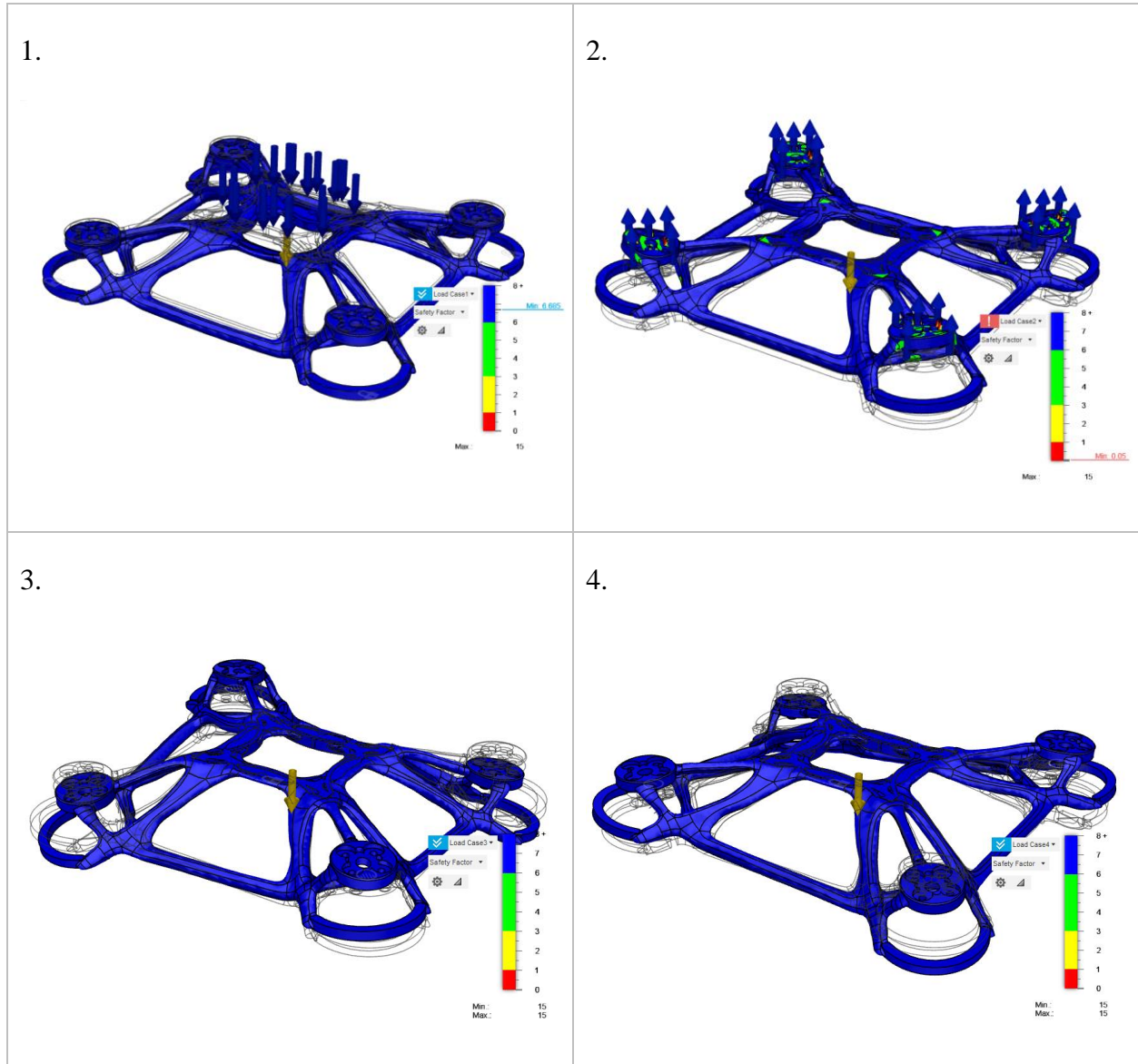


Table 17: Von Mises stress contour maps for the four load cases.

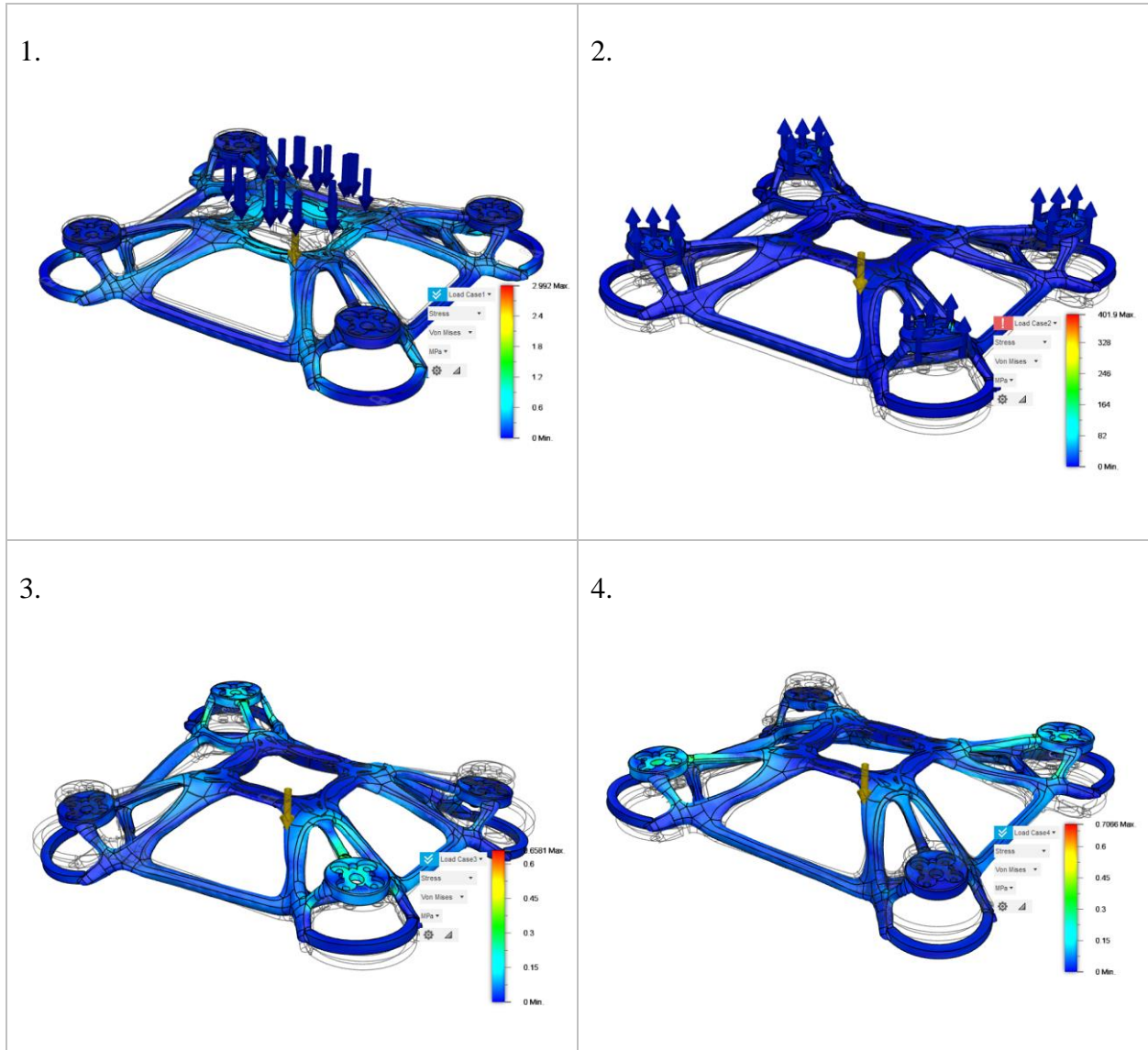
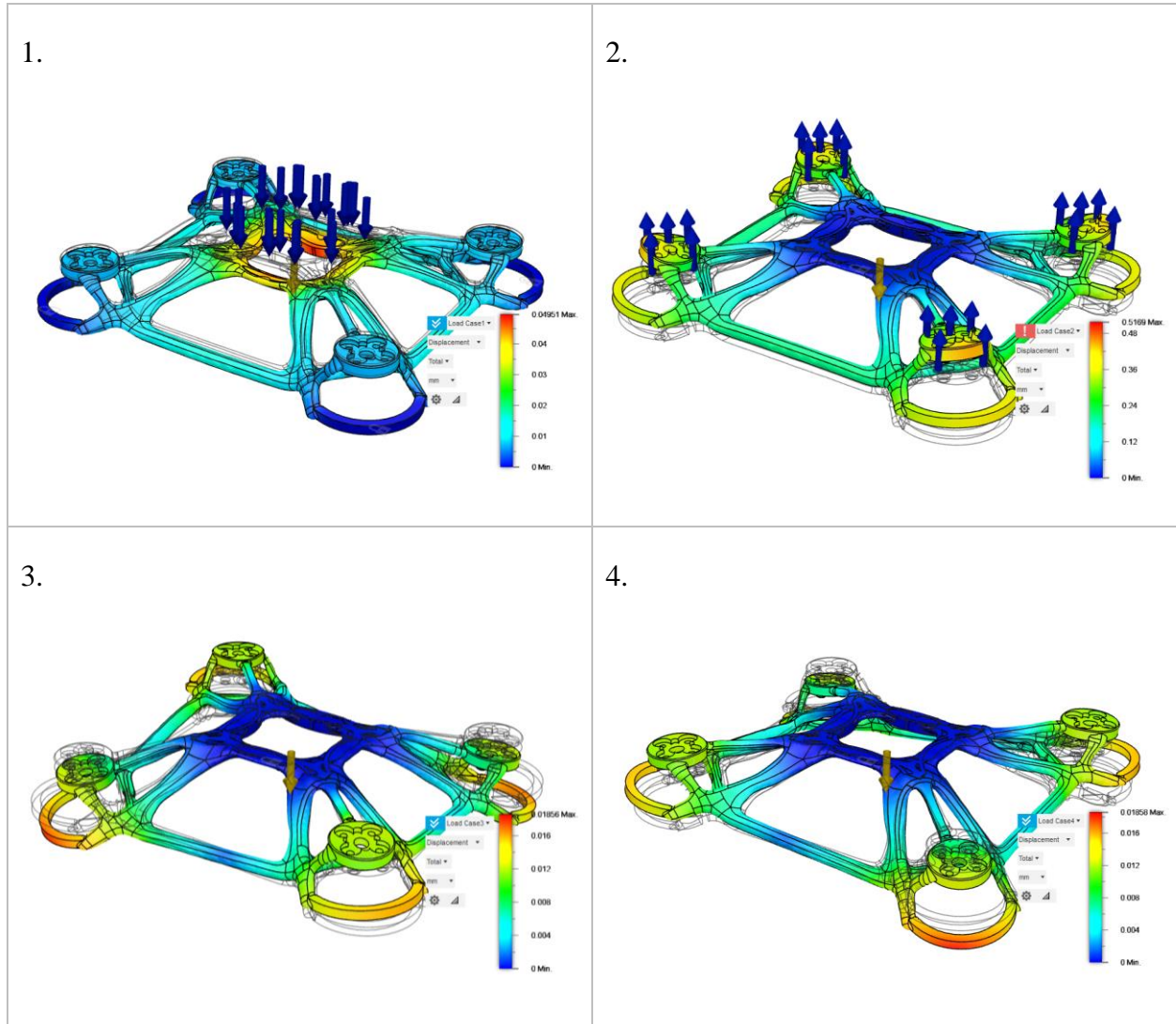


Table 18: Total displacement contour maps for the four load cases



The first two load cases generated trustworthy FEA results. The result for the second load case's minimum safety factor was determined to be an error because the localized sharp cusp where this safety factor is seen is not an applicable point of force. Figure 39 shows this phenomenon.

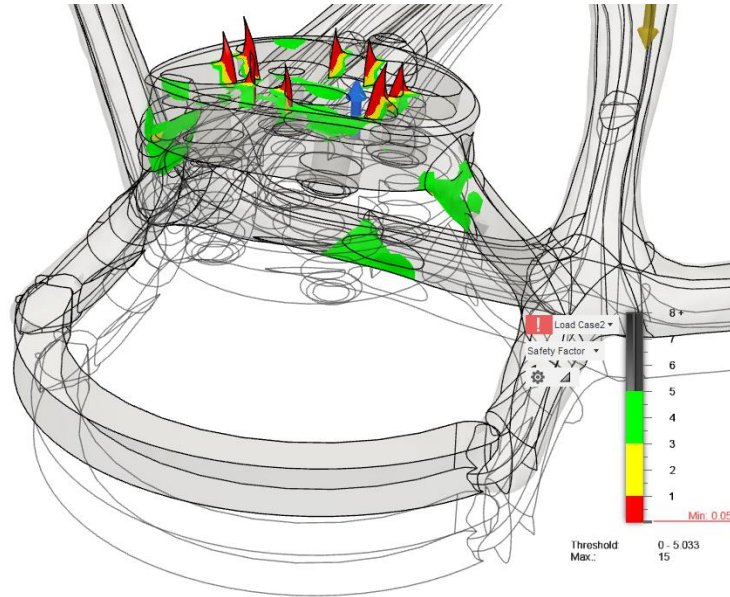


Figure 39: Localized region of extremely low minimum factor of safety for load case 2.

A more suitable value is approximately 5.00 since it better represents the actual distribution of load by a propulsion system. Nevertheless, the same problem arises when exploring maximum Von Mises stress and displacement.

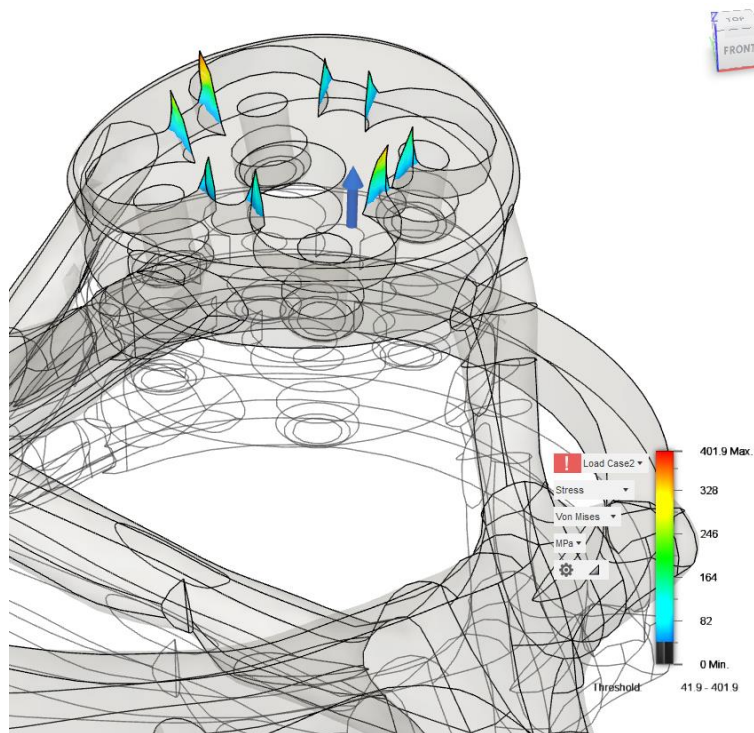
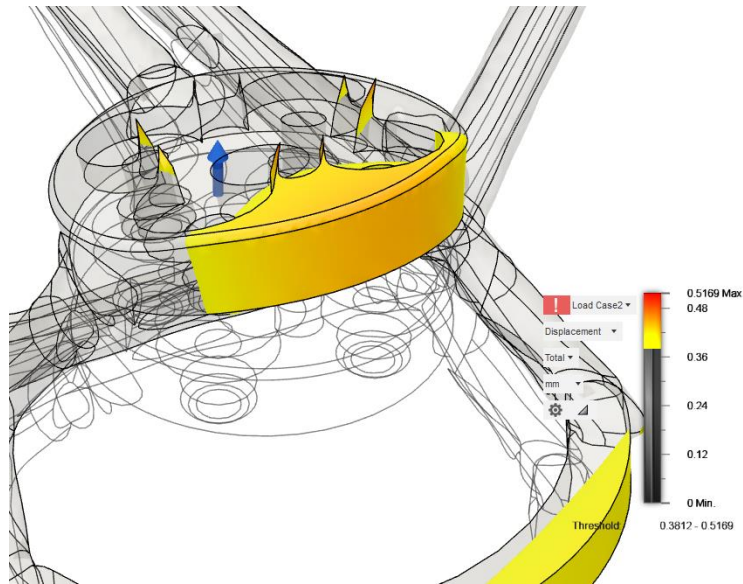


Figure 40: Localized region of extremely high Von Mises stress for load case 2.



*Figure 41: Localized region of extremely high displacement values for load case 2.*

Values that are more representative of the actual Von Mises stress and displacement that the drone experiences at these localized regions may be 41.9 MPa and 0.3812 mm respectively. It is not logically correct that these localized “cusps”/”spikes” are present in the case where propulsive systems generate upwards thrust. The most probable reason for this occurrence is that incorrect settings were applied when inducing the load. Perhaps the wrong face was chosen as the load location; it is also probable that the wrong load type was selected to represent propulsive thrust. The propulsive load, in a later study, should be applied in such a manner that considers the connection method between frame and components. In the future, more rigorous FEA set-up should be implemented to generate results more representative of real-life conditions.

Overall, generative design was able to create a structure suitable for the load cases applied to a small-scale drone imitating small hobbyist racing drones.

## 6.0 Physical Design

This section is concerned with sharing a general outlook of the manufactured prototype drone frame as well as data acquired during testing. In this section, the load cases applied to the design are explored through testing; in addition, the mass of the prototype and waste support material created by 3D printing was measured and is documented.

### 6.1 Observations

A prototype was manufactured via 3D printing using the Ultimaker Cura 5.1.0 slicer and an ORIGINAL PRUSA i3 3D printer at the FRAMES facility. Due to a limited print bed size, a  $\frac{3}{4}$  model was manufactured. In addition, due to the unavailability of PEEK and ABS, PLA plastic

was used to manufacture the prototype. A general outlook of the prototype may be seen in Figure 42.



*Figure 42: 3D printed generatively designed outcome 1.*

The printing process generally showed minimal signs of defects; the defects shown on the body of the drone include scarring, sharp corners, roughness, and loose fibres of plastic. Nevertheless, there is no sign of layer separation and improper connection between outline and infill discussed in Section 4.2. A picture showing the 3D printing process can be seen in Figure 43.

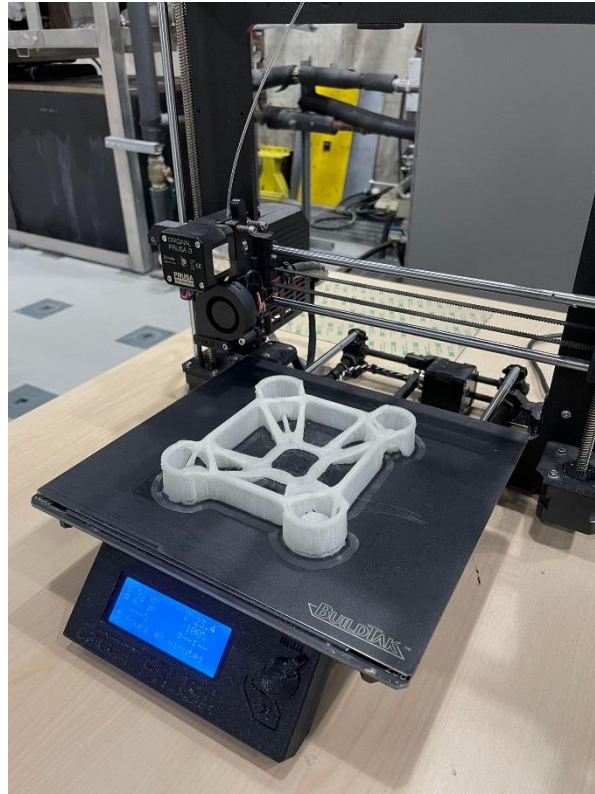


*Figure 43: 3D printing the drone body on the ORIGINAL PRUSA i3.*

## 6.2 Manufacturing Settings

The manufacturing conditions are important to consider when exploring the physical prototype since they strongly alter the performance of the product. The settings applied to the slicer (which is the software that transforms CAD drawings to G-code which is read by the printer), were those set by default to the “normal” resolution setting. A non-gradual infill density of 20% was used for the print. Moreover, “tree-structure” that does not build on top of material was used to support the part during printing. The “brim” type adhesion was used as the means of allowing strong initial adhesion to the plate. The temperature of the nozzle and bed were set to 210°C and 85°C respectively. The flow rate and printer speed were set to 100% which are the machine’s default settings. The manufacturing environmental conditions (temperature, pressure, and humidity) were not recorded though they may be taken to be similar to standard room temperature conditions. The predicted time to print was 6 hours and 22 minutes; the actual time was 5 hours and 48 minutes. Figure 44 demonstrates the splicing software’s rendition of the final print:

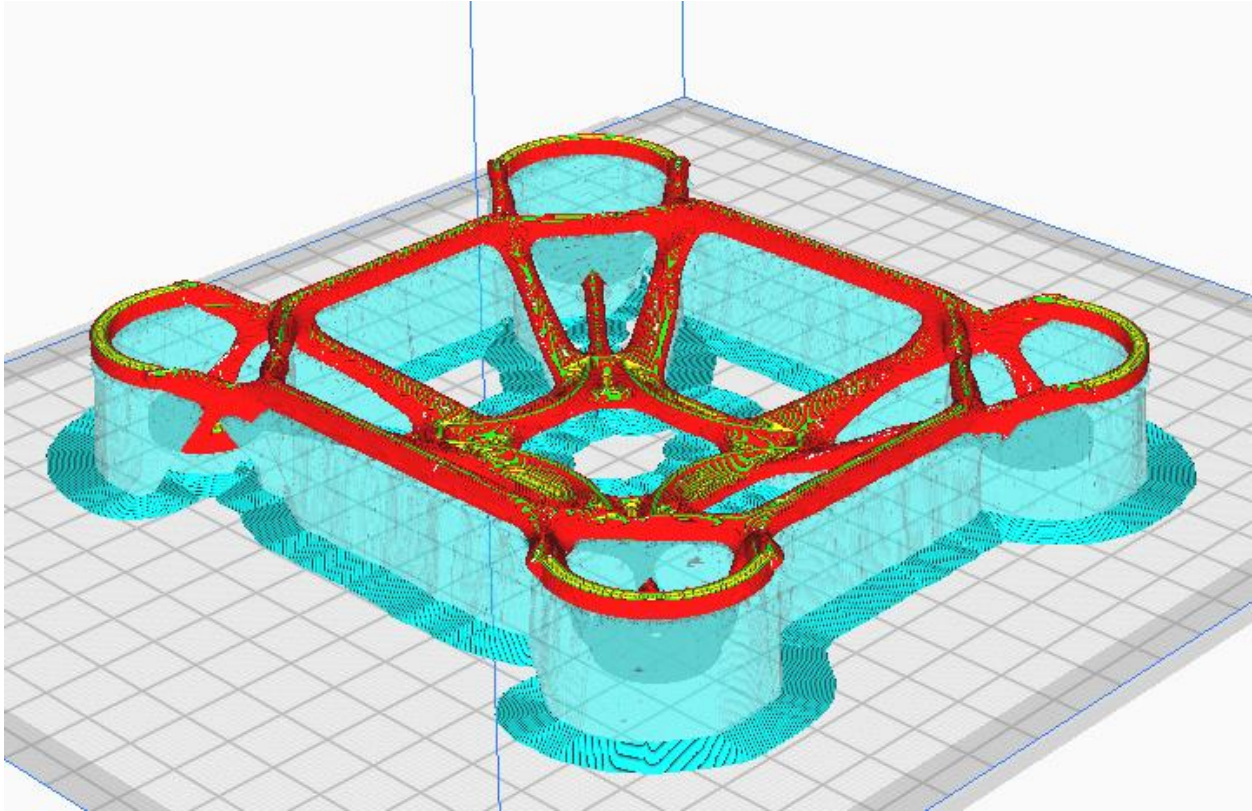


Figure 44: Preview of 3D print on the ORIGINAL PRUSA i3 printer on Ultimaker Cura 5.1.0.

### 6.3 Testing and Results

In order to measure the performance of the realized prototype as well as verify the claims made from FEA analysis presented in Section 5.3.3, load testing was conducted in the same directions and locations of each load case. The test set-ups for each test included a scale measuring weight. In each strength test, strength was measured quasi-statically to resemble static loads. A test for measuring the amount of waste material created in the manufacturing process was also conducted.

Table 19: Testing rigs corresponding to the load cases.

Load Case	1	2	3 and 4
Picture			

<b>Description</b>	The load is applied quasi-statically on the centre part of the frame whilst the landing gear rests on the scale. A manual pushing force increases the force experienced.	The load is applied quasi-statically on the centre part of the frame whilst the propulsion system mounts are held upwards. A manual pushing force increases the force experienced.	Tension is applied in the outwards direction by tying one end of the propulsion mount with a heavy weight (on the scale) and the other to a manual pulling force.
<b>Measurement</b>	The force may be taken from the scale reading minus the mass of the drone.	The force may be taken from the scale reading minus the mass of test stand and the drone.	The tension force may be taken by subtracting the final scale reading (after applying tension) from the initial reading (which is imposed by a heavy weight).

Load case 1 was the easiest to reproduce since it merely required a load applied evenly at the centre part of the drone frame. Load case 1 was not taken to failure since only one prototype was produced. The test that was taken to failure was load case 2 since the values presented from FEA were extremely apart from expected results; it was therefore curious to explore the maximum load for load case 2. Load cases 3 and 4 were investigated by tying a string to two opposite propeller mounts and pulling to create tension. It was assumed that no energy was lost within the string. For the same reason as load case 1, load case 3 was not taken to failure. The following table demonstrates the final results from testing as well as the percent error between the experimental and theoretical maximum static loads:

*Table 20: Load case results.*

<b>Load Case</b>	<b>Theoretical Maximum Static Load (N)</b>	<b>Maximum Static Load Found by Experimentation (N)</b>	<b>Pass/Fail</b>	<b>Percent Error (%)</b>
<b>1</b>	137 N	89 N	Fail	35
<b>2</b>	100 N	279 N	Pass	-
<b>3</b>	90 N	28 N	Fail	69
<b>and 4</b>				

The theoretical maximum static load was calculated by multiplying the minimum factor of safety by the load applied. Since the drone is characterised by having four arms, the net load experienced in load case 2 is four times the individual loads per arm. In addition, for load case 3, the net total

load (tension) is 2 times the individual loads per arm. Load case 2 was taken to failure due to its curious nature (since the theoretical values did not well represent the actual performance of the frame); the failure can be seen in Figure 45.



*Figure 45: Observed failure mode of load case 2.*

The failure case showed that all four propeller mounts failed in the two adjacent supports to the landing gear. Only two propeller mounts failed completely—fracturing in all three supports. The reason why two propeller mounts on the same side of the drone may be a result of uneven placement on the test fixture. It may also be due to inaccurate load placement on the drone centre body.

It is important to note that the load cases were applied to a +¼ size increased drone. Therefore, if the prototype survived the theoretical maximum loads applied to the larger drone, then the design of the drone succeeds. In addition, since PLA and ABS share similar tensile strengths and moduli of elasticity, then it can be said that if PLA succeeds the tests, then ABS also succeeds. Moreover, if the prototype is generally able to succeed in reaching/surpassing the theoretical loads, then it may be said that 3D printing as a means of manufacturing the drone frame is adequate. Load case 1 and load case 3 and 4 did not succeed in meeting the minimum loads and their respective safety factors. Nevertheless, the fact that load case 2 succeeded and was the only case in which load-until-failure was imposed suggests that, had the resources been available, all load cases would've passed the tests. A later study should involve a more organized test plan and custom-built test rigs to ensure the success of generative design in the three aspects.

The mass of the  $\frac{3}{4}$  prototype prior to post-processing and after post-processing was found to be 39.1g and 22.7g respectively. This indicates that the mass of waste material was 16.4g which is almost 42% of the total mass make-up. This large number proves that 3D printing may be a wasteful means of producing parts—especially for applications whereby large quantities of repeated products are desired. The theoretical volume of the generative design was provided by the Ultimaker Cura 5.1.0 splicer as 42g. The percent error between the theoretical and expected value was found as 45%. The load readings for each test are demonstrated in Appendix B.

## 7.0 Conclusion

Based on knowledge obtained through literature review, theoretical investigation, and experimentation, generative design proved to be a feasible means of advanced aerial drone design. Generative design, which uses a series of algorithms to explore various potential geometries for load distribution, provides a fast and efficient means of producing topology optimized structures; this is no less true in the application of drones. The literature review offered insight on previously studied means of drone frame optimization as well as inspiration for the methodology presented in this report. Independent study of three major aspects determining the success of the drone design—geometry, manufacturability, and material—concluded that the optimal frame type, manufacturing method, and material for achieving high performance were square, 3D printing (MEX/FFF), and PEEK respectively. Collectively integrating all acquired knowledge allowed for the creation of a generatively designed drone frame. The drone frame was analyzed using FEA and later verified via mechanical property testing of a small-scale, PLA, 3D printed prototype due to limitations in material availability and 3D printing build volume. Results demonstrated that only one of the four load cases succeeded in achieving quasi-static load factors-of-safety above the minimum factor-of-safety. Nevertheless, it was this load case (load case 2) that was tested to failure; the same was not done for the other tests which suggests the other load cases were not tested to their full potential. In general, it was found that the theoretical generative design made of ABS plastic in Fusion 360 had a minimum factor-of-safety of 37. For future studies, more sophisticated methods of testing the prototype should be implemented in the test plan. In addition, exploration of various generative outcomes with more concrete goals should be considered (e.g., achieving a certain impact strength for a given size and weight constraint). Other load cases that realistically represent drone behaviour in flight should also be implemented in generative design and FEA; this includes maneuvers such as sharp turns. More importantly, impact resistance of various drone frames should be explored since high-strain-rate forces from collisions are likely instances in drone flight. Acoustic stability and fatigue analysis should be conducted since vibrations caused by spinning rotors may damage the frame.

## References

- [1] B. Jones, “What is experimental design?,” JMP. [Online]. Available: [https://www.jmp.com/en\\_my/articles/what-is-experimental-design.html](https://www.jmp.com/en_my/articles/what-is-experimental-design.html). [Accessed: 05-Apr-2023].
- [2] J. Alkobi, “The evolution of drones: From military to hobby & commercial,” Percepto, 22-Feb-2022. [Online]. Available: <https://percepto.co/the-evolution-of-drones-from-military-to-hobby-commercial/>. [Accessed: 03-Apr-2023].
- [3] “DJI Naza-M v2/GPS Combo F450 ARF Kit + Landing Skid,” Aerialpixels. [Online]. Available: <https://aerialpixels.com/shop/arf-systems/dji-naza-m-v2gps-combo-f450-arf-kit-landing-skid/>. [Accessed: 03-Apr-2023].
- [4] J. Bright, R. Suryaprakash, S. Akash, and A. Giridharan, “Optimization of quadcopter frame using generative design ... - iopscience,” Optimization of quadcopter frame using generative design and comparison with DJI F450 drone frame, 2021. [Online]. Available: <https://iopscience.iop.org/article/10.1088/1757-899X/1012/1/012019>. [Accessed: 03-Apr-2023].
- [5] S. Sundararaj, K. Dharsan, J. Ganeshraman, and D. Rajarajeswari, “Structural and modal analysis of hybrid low altitude self-sustainable surveillance drone technology frame,” *Materials Today: Proceedings*, vol. 37, pp. 409–418, 2021.
- [6] A. O. MohamedZain, H. Chua, K. Yap, P. Uthayasurian, and T. Jiehan, “Novel drone design using an optimization software with 3D model, simulation, and fabrication in Drone Systems Research,” *Drones*, vol. 6, no. 4, p. 97, 2022.
- [7] J. M. Castiblanco, S. Garcia-Nieto, R. Simarro, and J. V. Salcedo, “Experimental study on the dynamic behaviour of drones designed for ...,” 03-May-2021. [Online]. Available: <https://journals.sagepub.com/doi/full/10.1177/17568293211005757>. [Accessed: 05-Apr-2023].
- [8] C. I. Basson, S. Hansraj, R. Stopforth, P. D. Mooney, R. Phillips, T. van Niekerk, and K. du Preez, “A review of Collaborated Educational Drone Development and Design at the BRICS 2018 future skills challenge,” 2019 Southern African Universities Power Engineering Conference/Robotics and Mechatronics/Pattern Recognition Association of South Africa (SAUPEC/RobMech/PRASA), 2019.
- [9] K. Fayazbakhsh, A. Abedian, B. D. Manshadi, and R. S. Khabbaz, “Introducing a novel method for materials selection in mechanical design using Z-transformation in statistics

for normalization of Material Properties,” *Materials & Design*, vol. 30, no. 10, pp. 4396–4404, 2009.

- [10] eFunda Inc. , “ Introduction to Compression Molding,” eFunda. [Online]. Available: [https://www.efunda.com/processes/plastic\\_molding/molding\\_compression.cfm](https://www.efunda.com/processes/plastic_molding/molding_compression.cfm). [Accessed: 10-Apr-2023].
- [11] S. Closures, “Plastic closures: Injection vs compression - what will you choose?,” *PLASTIC CLOSURES: INJECTION VS COMPRESSION – WHAT WILL YOU CHOOSE?*, 24-Sep-2020. [Online]. Available: <https://www.silgancls.com/compression-vs-compression-plastic-closures/>. [Accessed: 11-Apr-2023].
- [12] MACRODYNE, “Compression molding 101,” *Compression Molding 101*, 20-Jun-2022. [Online]. Available: <https://macrodynepress.com/compression-molding-101/>. [Accessed: 11-Apr-2023].
- [13] A. Cornejo, “Injection molding diagram.” Creative Commons Attribution-Share Alike 4.0 International, 25-Apr-2015.
- [14] M. F. Ashby, *Materials selection in mechanical design*. Oxford, United Kingdom: Butterworth-Heinemann, an imprint of Elsevier, 2017.
- [15] RapidDirect, “Compression molding vs injection molding: Which process is better,” *Compression Molding Vs Injection Molding: Which Method is Best for Your Application*, 08-Dec-2022. [Online]. Available: <https://www.rapiddirect.com/blog/compression-molding-vs-injection-molding/>. [Accessed: 11-Apr-2023].
- [16] R. Linke, “Additive Manufacturing, explained,” MIT Sloan, 07-Dec-2017. [Online]. Available: <https://mitsloan.mit.edu/ideas-made-to-matter/additive-manufacturing-explained>. [Accessed: 11-Apr-2023].
- [17] Parimala, B. C. P. Proxies, Multyashky.ru, Nani, Dadi, Z. Herron, and Jay, “How 3D printing works.,” *My 3D Concepts*, 28-Apr-2017. [Online]. Available: <http://my3dconcepts.com/explore/how-3d-printing-works/>. [Accessed: 11-Apr-2023].
- [18] Wohlersadmin, “The seven am processes,” *Wohlers Associates*, 30-Jun-2022. [Online]. Available: <https://wohlersassociates.com/terminology-and-definitions/the-seven-am-processes/>. [Accessed: 11-Apr-2023].
- [19] RapidDirect, “Injection molding defects: Causes and how to prevent them,” *Injection Molding Defects: Causes and How You Can Prevent Them*, 29-Sep-2022. [Online].

- Available: <https://www.rapiddirect.com/blog/injection-molding-defects/>. [Accessed: 11-Apr-2023].
- [20] Simplify3D, “Print Quality Guide,” Simplify3D Software, 21-Jun-2019. [Online]. Available: <https://www.simplify3d.com/resources/print-quality-troubleshooting/>. [Accessed: 11-Apr-2023].
- [21] M. von Übel, “3D printing materials – the ultimate guide,” 3D Printing Materials – The Ultimate Guide, 29-Nov-2022. [Online]. Available: <https://all3dp.com/1/3d-printing-materials-guide-3d-printer-material/>. [Accessed: 11-Apr-2023].
- [22] M. Spoerk, C. Holzer, and J. Gonzalez-Gutierrez, “Material extrusion-based additive manufacturing of polypropylene: A review on how to improve dimensional inaccuracy and warpage,” *Journal of Applied Polymer Science*, vol. 137, no. 12, p. 48545, 2019.
- [23] Essentra Components, “A comparison: Amorphous vs crystalline polymers,” Amorphous vs crystalline polymers | Essentra Components UK, 30-Jan-2023. [Online]. Available: <https://www.essentracomponents.com/en-gb/news/manufacturing/injection-moulding/the-difference-between-amorphous-and-semi-crystalline-plastics#:~:text=Crystalline%20polymers%20have%20large%20amorphous,semi%20crystalline%20plastics%20do%20not.> [Accessed: 12-Apr-2023].
- [24] Becky, “Best practices for bonding semi-crystalline thermoplastics " plastics decorating,” *Plastics Decorating*, 12-Aug-2019. [Online]. Available: <https://plasticsdecorating.com/articles/2015/best-practices-for-bonding-semi-crystalline-thermoplastics/>. [Accessed: 12-Apr-2023].
- [25] C. G. Amza, A. Zapciu, A. Eyþórsdóttir, A. Björnsdóttir, and J. Borg, “Mechanical properties of 3D printed composites with ABS/ASA substrate and glass fiber inserts,” *MATEC Web of Conferences*, vol. 290, p. 04002, 2019.
- [26] A. Afshar and R. Wood, “Development of weather-resistant 3D printed structures by multi-material additive manufacturing,” *Journal of Composites Science*, vol. 4, no. 3, p. 94, 2020.
- [27] J. Butt and R. Bhaskar, “Investigating the effects of annealing on the mechanical properties of FFF-printed thermoplastics,” *Journal of Manufacturing and Materials Processing*, vol. 4, no. 2, p. 38, 2020.
- [28] MakeShaper, “Comparing 3D printing filament features: ABS vs. Asa Filament,” *Makeshaper*, 30-Mar-2023. [Online]. Available: <https://www.makeshaper.com/post/comparing-3d-printing-filament-features-abs-vs-asa-filament.> [Accessed: 13-Apr-2023].





Ability to Retain Material Properties	12.9213	0.8	10.3371	0.7	9.04494	0.6	7.75281
Waste Material Production	9.55056	0.7	6.68539	0.8	7.64045	0.6	5.73034
Ability to Use Engineering Materials	13.4831	0.8	10.7865	0.7	9.4382	0.8	10.7865
<b>Final Score</b>	<b>100</b>		<b>68.4831</b>		<b>67.7528</b>		<b>70.4494</b>

Material Selection Process

Table 25: Method for determining material-property attribute weights according to [9].

#	Goals	Associated Property	Preference	Possible Decision																												Positive Decisions	Weighting Factors (α)		
				1	2	3	4	5	6	7	8	9	10	11	12	13	14	15	16	17	18	19	20	21	22	23	24	25	26	27	28				
1	Impact Resistance	Charpy Impact, Unnotched	Higher Value	2	3	3	3	3	3	3																								20	0.179
2	Mass	Density	Lower Value	2						3	3	3	3	3	2																			19	0.170
3	Stiffness	Modulus of Elasticity	Higher Value	1						1						1	2	3	3	2														13	0.116
4	Heat Resistance	Deflection Temperature at 0.46 MPa	Lower Value		1					1						3					2	3	3	2									15	0.134	
5		Maximum Service Temperature, Air	Higher Value			1					1						2				2				2	3	2							13	0.116
6	Strength	Tensile Strength, Ultimate	Higher Value				1					1					1				1			1			2	1					9	0.080	
7		Tensile Strength, Yield	Higher Value					1					1					1				1			1		1	2	1					8	0.071
8	Water Resistance	Water Absorption	Lower Value						1						2					2				2		2		2	3	3			15	0.134	

Table 26: Material properties of candidate materials [29].

Material	Acrylonitrile butadiene styrene	Poly lactic acid	Polyamide (Nylon 6)	Polypropylene (Impact Modified)	Polystyrene (Impact Modified)	Polycarbonate (Impact Modified)	Thermoplastic polyurethane (Glass Filled)	Acrylonitrile styrene acrylate	Polyethylene terephthalate glycol	Polyether etherketone (Unreinforced)	Polyetherketoneketone (Unreinforced)	Polyether Imide	Average	Standard Deviation	
Acronym	ABS	PLA	PA (Nylon 6)	PP (Impact Modified)	PS (Impact Modified)	PC (Impact Modified)	TPU (Glass Filled)	ASA	PETG	PEEK	PEKK	PEI			
Properties	Density g/cm <sup>3</sup>	1.08	1.28	1.13	0.93	1.05	1.20	1.45	1.08	1.26	1.34	1.28	1.38	1.20	0.141941122

Water Absorption	%	0.414	0.244	1.710	0.017	0.096	0.186	0.238	0.307	0.146	0.179	0.300	0.221	0.34	0.408532632
Tensile Strength, Ultimate	MPa	38.7	62.9	70.1	26.6	27.4	66.9	64.5	45.5	41.8	99.5	73.1	131	62.33	27.81713178
Tensile Strength, Yield	MPa	45.0	40.1	72.0	26.7	25.9	61.0	63.6	44.4	47.6	98.0	78.7	114.0	59.75	25.04876782
Modulus of Elasticity	GPa	2.05	2.27	1.47	1.32	1.99	2.36	2.58	2.13	2.59	4.00	3.32	7.68	2.81	1.561962933
Charpy Impact, Unnotched	J/cm <sup>2</sup>	15.4	2.64	21.0	3.65	7.70	6.00	12.7	7.81	6.94	10.9	4.87	3.20	8.57	5.084925119
Deflection Temperature at 0.46 MPa	°C	94.6	83	172	96.8	86.9	129	141	96.2	73.5	200	150	208	127.58	42.92804056
Maximum Service Temperature, Air	°C	89.2	179	116	122	106	122	141	96.2	67.3	263	257	180	144.89	58.0564905

Table 27: Z-transformation and performance index values.

Material	Acrylonitrile butadiene styrene	Poly lactic acid	Polyamide (Nylon 6)	Polypropylene (Impact Modified)	Polystyrene (Impact Modified)	Polycarbonate (Impact Modified)	Thermoplastic polyurethane (Glass Filled)	Acrylonitrile styrene acrylate	Polyethylene terephthalate glycol	Polyetheretherketone (Unreinforced)	Polyetherketoneketone (Unreinforced)	Polyetherimide		
Acronym	ABS	PLA	PA (Nylon 6)	PP (Impact Modified)	PS (Impact Modified)	PC (Impact Modified)	TPU (Glass Filled)	ASA	PETG	PEEK	PEKK	PEI		
Properties	Density	g/cm <sup>3</sup>	0.88	-0.53	0.53	1.96	1.09	0.03	-1.73	0.88	-0.39	-0.95	-0.53	-1.24
	Water Absorption	%	-0.19	0.23	-3.36	0.79	0.59	0.37	0.25	0.08	0.47	0.39	0.09	0.29
	Tensile Strength, Ultimate	MPa	-0.85	0.02	0.28	-1.28	-1.26	0.16	0.08	-0.61	-0.74	1.34	0.39	2.47
	Tensile Strength, Yield	MPa	-0.59	-0.78	0.49	-1.32	-1.35	0.05	0.15	-0.61	-0.49	1.53	0.76	2.17
	Modulus of Elasticity	GPa	-0.49	-0.35	-0.86	-0.96	-0.53	-0.29	-0.15	-0.44	-0.14	0.76	0.32	3.12
	Charpy Impact, Unnotched	J/cm <sup>2</sup>	1.34	-1.17	2.44	-0.97	-0.17	-0.50	0.81	-0.15	-0.32	0.46	-0.73	-1.06
	Deflection Temperature at 0.46 MPa	°C	0.77	1.04	-1.03	0.72	0.95	-0.03	-0.31	0.73	1.26	-1.69	-0.52	-1.87
Maximum Service Temperature, Air	°C	-0.96	0.59	-0.50	-0.39	-0.67	-0.39	-0.07	-0.84	-1.34	2.03	1.93	0.60	
Performance Index		0.1886	-0.1548	-0.1627	0.0075	0.0242	-0.1018	-0.1650	-0.0100	-0.1572	0.2872	0.0696	0.1744	

Rank	2	9	11	6	5	8	12	7	10	1	4	3
------	---	---	----	---	---	---	----	---	----	---	---	---

## Appendix B

### Load Case 1



*Figure 46: Load case 1 final reading.*

### Load Case 2



*Figure 47: Load case 2 final reading (brought to failure).*

## Load Case 3 and 4



*Figure 48: Load cases 3 and 4 final reading.*

Mass



*Figure 49: Prototype and waste material mass.*



Figure 50: Prototype mass after post-processing.

## Appendix C

Input

%% Initialization

% Samuel Osorio Marino

% Toronto Metropolitan University (Formally Ryerson University)

% PRELIMINARY DRONE LOAD CALCULATIONS THROUGH PULL-OUT

clc

clear

close all

%% Parameterization

% All units in this study are SI units; that is: meters, seconds,

% kilograms, newtons. In addition, an increase in height is taken as

% positive.

vi = -0; % Set initial velocity in m/s

```

g = -9.81; % m/s^2
hi = -7.5; % Set height of fall initialization in m
hl = 1; % Set offset from ground that the drone must not fall under

time_allocated_reaction = 0.5; % Allocate time for system reaction in s
time_allocated_moment = 0.5; % Allocate time for re-orientation in s

m_drone = 1; % Set mass of drone in kg
num_arms = 4; % Set number of arms (number of rotors)
length_arm = 0.084; % Set length of arms (meters)

%% Part Nulla - I: Initial Drop
% The initial drop information describes the start time and height from
% which the drone is dropped. Changing the initial velocity is also
% possible

time_remain_res_0 = time_remain(vi,hi,g);
distance_remain_res_0 = distance_remain(vi,time_remain_res_0,g);

fprintf('At phase 0, the time and distance remaining are: \n')
disp(time_remain_res_0);
disp(abs(distance_remain_res_0));

%% Part I - II: Reaction
% Time is allocated for latency in reaction time. The drone undergoes free
% fall in this phase.

time_remain_res_1 = time_remain(vi,hi,g) - time_allocated_reaction;
distance_remain_res_1 = (distance_remain(vi,time_remain_res_0,g)) -
(distance_remain(vi,time_allocated_reaction,g));
final_velocity_res_1 = final_velocity(vi,time_allocated_reaction,g);

fprintf('At phase 1, the time and distance remaining are: \n')
disp(time_remain_res_1);
disp(abs(distance_remain_res_1));

%% Part II - III: Moment
% Assuming that the drone is oriented in such a manner that it cannot
% provide direct upwards thrust, a moment must be created by activating one
% or more turbines. Doing so takes time and therefore contributes to the

```

% time falling. In this phase of the fall, it is assumed that the turbines  
 % can generate thrust in only one direction and may not reverse direction  
 % of spin. In addition, it is assumed that no upwards thrust is provided in  
 % the re-orientation.

```
time_remain_res_2 = time_remain(vi,hi,g) - time_allocated_reaction - time_allocated_moment;
distance_remain_res_2 = (distance_remain(vi,time_remain_res_0,g)) -
(distance_remain(vi,time_allocated_reaction,g)) -
(distance_remain(final_velocity_res_1,time_allocated_moment,g));
final_velocity_res_2 = final_velocity(vi,time_allocated_reaction + time_allocated_moment,g);
```

```
fprintf('At phase 2, the time and distance remaining are: \n')
disp(time_remain_res_2);
disp(abs(distance_remain_res_2));
```

%% Part III - IV: Landing

% Room for safety in landing is provided in this phase. A set amount of  
 % space from the ground is parameterized in order to find the acceleration  
 % necessary after all phases in order to decelerate the drone at the  
 % specified distance from the ground.

```
a = (-final_velocity_res_2.^2)/-(2*(abs(distance_remain_res_2) - hl));
time_remain_res_3 = time_remain(final_velocity_res_2,distance_remain_res_2 + hl,a);
```

```
fprintf('At phase 3, the acceleration required to stop the drone at the specified height away from
the ground is: \n')
disp(a);
fprintf('The time for this maneuver is: \n')
disp(real(time_remain_res_3(1)));
```

%% Test

% To verify that all calculations were done correctly, the distance  
 % remaining going forwards must be equivalent to that which was defined by  
 % the user.

```
distance_remain_res_3 = (distance_remain(vi,time_remain_res_0,g)) -
(distance_remain(vi,time_allocated_reaction,g)) -
(distance_remain(final_velocity_res_1,time_allocated_moment,g)) -
(distance_remain(final_velocity_res_2,real(time_remain_res_3(1)),a));
```

```

%% Force
% With acceleration known, as well as the weight of the drone, it is
% possible to calculate the force that each arm experiences.

thrust_tot = m_drone*a;
thrust_per_arm = thrust_tot/num_arms;
thrust_per_arm_ORI = thrust_tot/(num_arms - 1);

fprintf('The upwards force that each arm experiences during the upwards thrust in deceleration
is: \n')
disp(thrust_per_arm);

fprintf('With one rotor inoperable, the upwards force that each arm experiences during the upwards
thrust in deceleration is: \n')
disp(thrust_per_arm_ORI);

body_ang_vel = pi/time_allocated_moment;
body_tip_speed = body_ang_vel*length_arm;
centri_force = m_drone*(body_tip_speed.^2)/(length_arm);
fprintf('Given the time to re-orient, the centripetal force is: \n')
disp(centri_force);

%% Functions

function time_remain_res = time_remain(vi,d,a)
syms t
kin_1 = d == (vi*t) + (0.5*a*t.^2);
S_t_eqn = solve(kin_1,t);
S_t_sol = double(S_t_eqn);
S_t_sol_pos = S_t_sol(S_t_sol >= 0);
time_remain_res = S_t_sol_pos;
end

function distance_remain_res = distance_remain(vi,t,a)
distance_remain_res = (vi*t) + (0.5*a*t.^2);
end

function final_velocity_res = final_velocity(vi,t,a)
final_velocity_res = (vi) + (a*t);
end

```

Output

*At phase 0, the time and distance remaining are:*

1.2365

7.5000

*At phase 1, the time and distance remaining are:*

0.7365

6.2737

*At phase 2, the time and distance remaining are:*

0.2365

2.5950

*At phase 3, the acceleration required to stop the drone at the specified height away from the ground is:*

30.1681

*The time for this maneuver is:*

0.3252

*The upwards force that each arm experiences during the upwards thrust in deceleration is:*

7.5420

*With one rotor inoperable, the upwards force that each arm experiences during the upwards thrust in deceleration is:*

10.0560

*Given the time to re-orient, the centripetal force is:*

3.3162

>>